

# **Numerical Analysis of Aerodynamic Characteristics of Multi-Element S1223 Airfoil**

by

**Al Mamun Arabi**

**Roll No. 1705012**



DEPARTMENT OF MECHANICAL ENGINEERING  
KHULNA UNIVERSITY OF ENGINEERING & TECHNOLOGY  
KHULNA-9203, BANGLADESH  
FEBRUARY, 2023

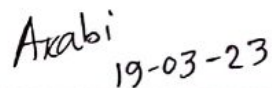
## Declaration

This is to certify that the thesis work entitled "Numerical Analysis of Aerodynamic Characteristics of Multi-Element S1223 Airfoil" has been carried out by Al Mamun Arabi, Roll No. 1705012 in the Department of Mechanical Engineering, Khulna University of Engineering and Technology, Khulna, Bangladesh. The above thesis work or any part of this work has not been submitted anywhere for the award of any degree or diploma.



---

Dr. Md. Helal-An-Nahyan



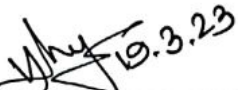
---

Al Mamun Arabi

## **Approval**

This is to certify that the thesis work submitted by (Al Mamun Arabi, Roll No. 1705012) entitled "Numerical Analysis of Aerodynamic Characteristics of Multi-Element S1223 Airfoil" has been approved by the board of examiners for the partial fulfilment of the requirements for the degree of Bachelor of Science in the Department of Mechanical Engineering, Khulna University of Engineering & Technology, Khulna, Bangladesh in February, 2023.

### **BOARD OF EXAMINERS**

1.  19.03.23  
(Supervisor)

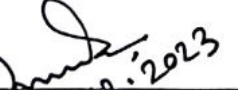
Dr. Md. Helal-An-Nahiyan

Professor

Department of Mechanical Engineering

Khulna University of Engineering & Technology

Khulna-9203, Bangladesh

2.  19.03.2023  
(External Member)

Dr. Sobahan Mia

Professor

Department of Mechanical Engineering

Khulna University of Engineering & Technology

Khulna-9203, Bangladesh

## **Acknowledgment**

The author wants to express his gratitude and gratefulness to Allah Subhanahu Wa Ta'ala for His kindness and mercy on me to complete this thesis work.

I would like to express my sincere gratitude, recognition, and special thanks to my supervisor, Dr. Md. Helal-An-Nahiyani, Department of Mechanical Engineering, Khulna University of Engineering and Technology, Khulna. This work would not have been possible without his encouragement and supervision.

- Al Mamun Arabi

## **Abstract**

This study presents two-dimensional numerical investigations of aerodynamical characteristics such as lift coefficient, drag coefficient, pressure distribution over a surface of an airfoil of Selig-S1223 at low Reynolds number. These numerical simulations were carried out by using ANSYS Fluent to determine the aerodynamic properties of a 2-D Selig S1223 airfoil at various angles of attack ( $\alpha$ ) at a fixed Reynolds number (Re), equal to  $4.2 \times 10^5$ . After this, different configurations of airfoils were simulated to analyse the aerodynamic characteristics with a purpose to determine better configuration. Higher angles of attack were shown to enhance both the lift and drag coefficients; however, the lift coefficient starts to decrease at an angle of attack of  $13^\circ$ , which is referred to as stalling. The highest lift-to-drag ratio  $C_L/C_D$  was experienced as 29.642 for varying angle of attack in order of  $7^\circ, 28^\circ, 46^\circ$ .

## List of Contents

### Contents

Declaration .....	i
Approval .....	ii
Acknowledgment .....	iii
Abstract .....	iv
List of Contents.....	v
Contents .....	v
List of Figures .....	vii
List of Tables .....	ix
CHAPTER I.....	1
1.1 General .....	1
1.2 Problem Description.....	5
1.3 Objectives.....	5
CHAPTER II.....	6
2.1 Literature Review:.....	6
CHAPTER III .....	12
3.1 Airfoil .....	12
3.2 CAD Model .....	12
3.3 Computational Method.....	13
CHAPTER IV .....	15
4.1 Governing Equations.....	15
4.2 SST k- $\omega$ Model.....	16
4.3 Computational Domain and Boundary Conditions .....	17
4.4 Mesh Generation for Baseline Airfoil.....	18
4.5 Mesh Independence Test for Baseline airfoil.....	19

4.6 Mesh Generation for Multi-Element Airfoil cross section.....	19
4.7 Mesh Independence Test for Multi-element Airfoil cross section.....	21
4.8 Numerical Set-up.....	22
4.9 Validation.....	23
CHAPTER V .....	24
5.1 Changes of Negative Lift Coefficient and Drag Coefficient for baseline airfoil .....	24
5.2 Analysis of multi-element airfoil cross section.....	27
5.3 Comparison of better aerodynamic properties between two configurations.....	31
5.4 Velocity contours: .....	34
5.5 Pressure contours: .....	36
CHAPTER VI .....	40
6.1 Conclusion.....	40
References .....	41

## List of Figures

Figure 1. 1 Picture of an FSAE car [6] .....	2
Figure 1. 2 Basic diagram for lift and drag for an airfoil [10] .....	3
Figure 3. 1 S1223 airfoil's geometry .....	12
Figure 3. 2 CAD geometry for numerical analysis .....	12
Figure 4. 1 Computation domain with boundary conditions .....	17
Figure 4. 2 Mesh inside the entire domain.....	18
Figure 4. 3 Mesh around the S1223 airfoil .....	18
Figure 4. 4 Variation of negative lift coefficient with number of elements .....	19
Figure 4. 5 Meshing for multi-element airfoil cross section.....	20
Figure 4. 6 Detailed view of mesh for r multi-element airfoil cross section with inflation layer.....	20
Figure 4. 7 Variation of negative lift coefficient with number of elements .....	21
Figure 4. 8 Comparison between the variation of $C_L$ Vs $\alpha$ with the result of Ali Doosttalab et al. [34] .....	23
Figure 5. 1 Negative Lift coefficient ( $C_L$ )Vs Angle of Attack ( $\alpha$ ).....	24
Figure 5. 2 Drag coefficient ( $C_D$ ) Vs Angle of Attack ( $\alpha$ ).....	25
Figure 5. 3 ( $C_L / C_D$ ) Vs Angle of Attack ( $\alpha$ ) .....	25
Figure 5. 4 Negative lift vs angle of attack.....	26
Figure 5. 5 Drag vs angle of attack .....	27
Figure 5. 6 The ratio of $C_L / C_D$ for different sets of angles of attack (Degree) .....	27
Figure 5. 7 Negative lift for different configuration.....	28
Figure 5. 8 Drag for different configuration .....	29
Figure 5. 9 $C_L$ for different configuration.....	29
Figure 5. 10 $C_D$ for different configuration.....	30
Figure 5. 11 Comparison of the $C_L / C_D$ ratio for different velocities .....	31
Figure 5. 12 Comparison of the $C_L$ for different velocities .....	31
Figure 5. 13 Comparison of the $C_D$ for different velocities .....	32
Figure 5. 14 Comparison of the Drag for different velocities.....	32

## List of Tables

Table 4. 1 Meshing parameters .....	21
Table 4. 2 Numerical Setup and Solver Settings .....	22
Table 4. 3 Solution Methods .....	22
Table 4. 4 Solution controls .....	23

## CHAPTER I

### Introduction

#### 1.1 General

Aerodynamics is the study of how relative motion between air molecules and body surfaces affects the outcomes. It is crucial to comprehend how air flows around moving objects because, among other things, air flow may be controlled to an aircraft's advantage as well as that of a wind turbine, a drone, and many other devices. By using fundamental physics equations like Newton's laws and the Navier-Stokes equation, aerodynamics focuses on researching this phenomenon [1]. To determine the shape of an item, such as the airfoil or wing cross-section in the case of an airplane, is important in order to examine the aerodynamic profile of that thing. The cross-sectional shape of a wing or blade (of a turbine, rotor, or propeller) that is introduced into an airstream to produce beneficial aerodynamic forces is known as an airfoil. Both empirically and computationally can be used to study the aerodynamic profile of an airfoil. In the experimental method, an airfoil (or wing model) is placed in a controlled wind tunnel while the velocity and pressure distribution around it is monitored to determine the aerodynamic properties of the airfoil. The identical experiment can be carried out computationally using a CFD code [2].

Formula SAE is an international competition for students held annually which is focused on designing and manufacturing formula styled open wheeled racing car. The evaluation of the car designing goes through a process which includes their performance in both static and dynamic events. Although for safety issue, the average velocity is intended to be kept low within standard limit. For better performance some key parameters are considered such as weight reduction, decreasing fuel consumption, increasing downforce etc. Aerodynamic devices like front and rear wings are used to increase the downforce experienced by the car to increase traction between tyres and the road specifically at the moment of cornering at higher speed. Downforce is considered very useful in case of maintaining balance of the vehicle from air pressure in case of turning.

Usually, positive lift is generated by a car body which retards the high-speed cornering ability. Aerodynamic components like front and rear wing generate negative lift that is helpful for this

phenomenon. The prime concern is to manufacture and assemble a vehicle which will utilize as much downforce as possible, as a result will lead to better timing during the competition [3].

In the stratosphere, airfoil for an aircraft propeller typically operate in the  $2 \times 10^5$  to  $5 \times 10^5$  Reynolds number range, which is within the low Reynolds number region. The maximum lift-to-drag ratio of common airfoil rapidly decelerates, as does the non-linear phenomenon of symmetrical airfoils at small attack angles, particularly around  $0^\circ$ , among other novel properties of an airfoil under low Reynolds number conditions [4]. Sir George Cayley made the early 1800s-era discovery that a curved surface creates more lift than a flat plate of a comparable size. Using an airfoil is the most efficient way to accomplish this [5].

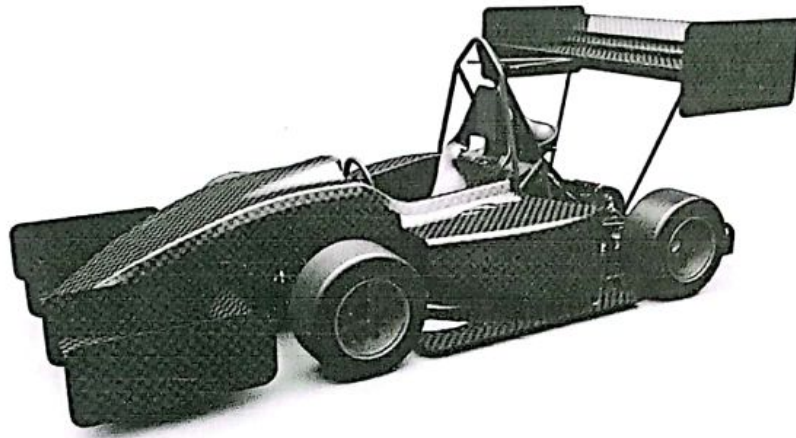


Figure 1. 1 Picture of an FSAE car [6]

The aerodynamic profiles of the Selig S1223 airfoil are determined in this study using a CFD technique. The three primary components of the CFD programs are the Pre-processor, Solver, and Post-processor. In the recent past, CFD has been the method of choice in the aerospace, automotive, and many industrial components. Because it costs less than an experimental procedure and produces more precise findings, CFD is widely employed in the field of aerodynamics. In order to accurately simulate the flow over an airfoil, it is crucial to understand the transition from laminar to turbulent flow [7]. The quick development of CFD (Computational Fluid Dynamics) technology provides us with a significant chance and ease to perform such tasks. Aerodynamic issues are frequently thought of as being solvable using the RANS (Reynolds-Averaged Navier-Stokes) approach. The flow is typically considered to be totally in a turbulent condition in traditional RANS turbulence models. On the airfoil's surface, nevertheless, the transition from laminar to turbulent happens. Taking the transition into account, then, can, in some cases, improve the precision of numerical simulations [8].

Lift and drag are two fundamental aerodynamic forces that play a crucial role in the design and operation of a wide range of vehicles, including airplanes, cars, and boats. Understanding the principles of lift and drag is essential for engineers and designers in various fields to optimize the performance, efficiency, and safety of their products. A pressure force perpendicular to the upper and lower surfaces and a shear force parallel to the surfaces are both exerted by the fluid flow across the airfoil. The area of interest is the product of these two forces. Lift force is the normal component of the force, and drag is the force acting in the direction of the flow [9].

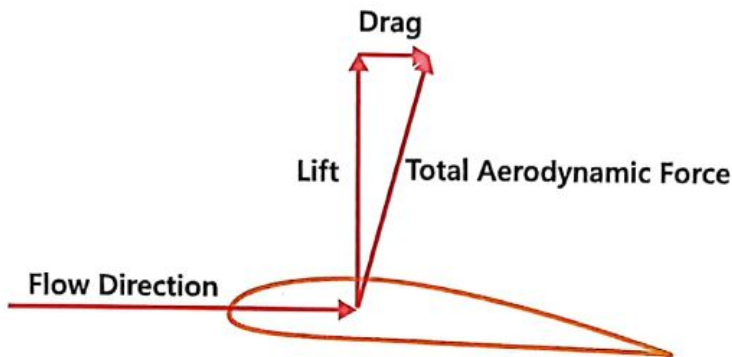


Figure 1. 2 Basic diagram for lift and drag for an airfoil [10]

In aerodynamics, most vital elements are downforce, drag force, lift and co-efficient of drag and lift. Downforce is responsible for pushing the car so that the car obtains more grip with the ground and the slip decreases. On the other hand, lift is the load tends to push the vehicle up as high-speed air flow passing from the front of the car. For formula cars, the lift generally happens from the bottom of the car. These phenomena increase slip between the wheels and the ground. As a result, aerodynamic performance of the car is lessened. In addition, drag force is one vital aspect in aerodynamics. Drag force is defined as the load tends to push the car at opposite direction of the velocity. Undesirable drag with downforce reduces car speed. Along with this, drag co-efficient is significant as it is affected by body and aerodynamic devices. Drag co-efficient is a measurement of the resistance created by an object in a fluid domain. It is important to ensure the minimum drag contributed by the wings to reduce the engine losses in overcoming drag. Additional aerodynamic devices are used in order to decrease lift and drag force which are proportional to each other. Also, there may occur complexity for example, addition of front wing helps to reduce lift but in the mean time they may also increase drag force. Therefore, it is important to make a design as efficient as possible to obtain the best result considering all these criteria [11].

The angle of attack of the wing, defined as the angle between the wing and the horizontal plane, is another significant design parameter that influences the amount of downforce created by the wing. In most cases, the angle of attack can be altered, allowing the driver to modify the car's handling characteristics to the track's circumstances. The design and functionality of rear wings for FSAE cars have been the subject of numerous studies. It has long been known that multi-element wings with a low aspect ratio provide the most downforce. Overall, the rear wing is a critical element in the design of FSAE race vehicles, and its size, shape, and angle of attack must be carefully tuned to produce the appropriate performance and handling qualities.

The Formula SAE contests involve automobiles that are judged on both their design in static events and their actual performance in dynamic events, with a 22 km endurance race serving as the competition's grand finale. Competition speeds are considered low-velocity racing; top straight-away speeds can reach roughly 100 to 105 km/hr, with average speeds ranging from 40 to 48 km/hr. While a typical track features at least three straight-away portions, the majority of the endurance lap is made up of slalom sections. Although most racing takes place at modest speeds, aerodynamics is heavily incorporated into vehicle design [12].

The rear wing will have a 2D cross section of multiple inverted airfoils co-ordinated in desired angle of attack order at the back side of the vehicle. Airfoils behave much differently in close proximity to the ground than they do in free-stream air; pressure/velocity changes of flowing air due to the ground are called "ground effects". A primary study will be about the effects of angle of attack, conducted on airfoil that have a chord length of  $c = 0.5$  m. A second study that is discussed is about the airfoil's behaviours according to different sets of angles of attack and the same chord length,  $c = 0.5$  m, 0.2 m and 0.15 m without considering the ground effect.

## **1.2 Problem Description**

It is now widely accepted that aerodynamics plays a significant influence in an open wheel racing car's efficiency and performance, even when the car is traveling at slow track speeds, as is the case with FSAE cars. Using the airflow around it, a well-designed aerodynamic car may deliver as much vertical to ground force as feasible while keeping air resistance force at a minimum. Downforce or negative lift is the name given to the vertical force, and Drag is the name given to the opposing force. By doing this, the tires' grip and performance improve, the automobile can turn at faster speeds, and because the air resistance is lowered, the fuel economy is also improved.

Many FSAE Competition tracks are made up mostly of numerous tight curves rather than long straights in order to keep vehicle speeds low for safety reasons. This fact made the majority of the FSAE teams understand that improving their cars' cornering performance is the key to winning the race. Due to the huge difference in cornering speed, an FSAE car that incorporates aerodynamic devices can significantly lower its lap time, which increases the importance of an efficient aerodynamic design.

## **1.3 Objectives**

The primary goals of this study are:

- i. To investigate the aerodynamic properties of a 2-D Selig S1223 airfoil at various angles of attack ( $\alpha$ ) and fixed chord length.
- ii. To investigate the aerodynamic properties of various configurations of multiple S1223 airfoils according to different configurations of angles of attack.
- iii. To compare the results to create a better understanding of airfoil layout from various perspectives.

## CHAPTER II

### Literature Review

#### 2.1 Literature Review:

A details study by Ioannis Oxyzoglou represents the use of CAD tools and computational fluid dynamics to design and build the aerodynamic package for Centaurus Racing Team's 2016 Formula Student race vehicle (Thireus 277). (CFD). It also looks into how aerodynamics affects how the vehicle performs and behaves in relation to the rules of the Formula Student competition. By examining the relationship between the CFD findings of the automobile model and their lap-time simulated equivalent, the development processes are assessed and placed into perspective. The nosecone, two sidepods, an undertray, a front wing, and a rear wing make up the aerodynamic package. The study outlines each stage of component design and optimization to achieve the desired outcomes and maximize the amount of performance-improving aerodynamic downforce produced by the aerodynamic package while keeping drag force at a minimum. The considered parameters are downforce and drag generated at different case for speeds, downforce generated at different corner radius, downforce generated at different parts of the track, vehicle speed at different corner radius, percent of Engine throttle at different corner radius etc [13].

An experimental and numerical study by Kaviem and Chelven states that wing-ground collision is an important aerodynamic problem in practical life. Interference with ground remarkably changes the aerodynamic characteristics of the wings. In this study, collision with the ground of 2D airfoil section was investigated both experimentally and numerically. The experiment was performed in a wind tunnel including a series of investigations. A wing model from NACA4412 airfoil section was fabricated using CNC machine. Fluent software was used for numerical simulations. The result represented that aerodynamic properties are significantly affected when wing is close to the ground. The validation of numerical analysis was done by comparing with previous and recent experimental data. This research found out that superior performance of NACA4412 airfoil with ground effect is obtained for angles of attack 4° to 8° [14].

Similar wings are used in racing cars and airplanes. The main difference is airfoils are inverted and operated in high ground effect in case of racing cars. Peters et al investigated aerodynamic properties of NACA0012 and DHMTU airfoils. They used wind tunnel while considering

ground effect. The study presented that the drag increases with decreasing altitude in case of the DHMTU airfoil. While considering the ground effect, superior lift to drag ratio was generated by DHMTU aerofoil. As a result, their study represented that lift to drag ratio is superior at low angle of attack [15].

Dalhberg proposed the idea of an inverse aerofoil design for FSAE cars. This study contains a developing procedure for the aerodynamic package of a formula student car with computational fluid dynamics. A wing in ground proximity was experimented in a wind tunnel along with simulated counterpart. The correlation between the experimental data and numerical data evaluated the method of the study [16].

A study of Wordley and Sanders was based on the down force calculation also with the understanding of balancing aerodynamic forces generated by the front and rear wings. The study aimed to generate maximum downforce within acceptable limit of increased drag and reduced top speed. The effect of the wings on the performance of a FSAE car was predicted. The study has been shown that addition of wing should result in significantly higher cornering potential along with higher acceleration potential. As a result, addition of wing significantly enhanced the performance of the car in dynamic events [17].

Zhaowen Deng et al completed analysis of aerodynamic characteristics of a FSAE car body with and without aerodynamic devices. CATIA was used to create the CAD model. The authors checked the performance parameters of, co efficient of lift and co efficient of drag for different values and selected their desirable wing profile. The simulation process was done for with and without aerodynamic devices. Using the aerodynamic devices significantly increased the performances, the lift and downforce was much higher with using aerodynamic devices [18].

A Siddharth Reddy et al worked on front and rear wing of an FSAE car to design and develop them. comparison of drag and lift forces was shown for multiple aerofoils based on their arrangements. The authors considered multiple aerofoil designs and based on their characteristics' best suited design was selected. Simulations were carried out to obtain desired outcome. The wing placement, angle of attack and chord length was fixed based on simulation. Solidworks was used to create the CAD geometries and Ansys fluent was used for simulation [11].

Francesco Mariani et al aimed to develop the external fluid dynamics of a prototype of the FSAE race car form University of Perugia. For the first part of study, they studied the prototype experimentally in a wind tunnel and then compared the results with obtained results from

simulation. The overall result obtained from the study can be said as the stability was improved for using front and rear wing [19].

Sneha Hetawal et al conducted this study to reduce the drag force and enhance the stability of the vehicle. The aerodynamic study was done in ANSYS Fluent software. The required CAD models were designed in SOLIDWORKS 2013. For all three models, a low-speed CFD analysis of the flow over the car was conducted at a speed of 25 m/s. The end result cleared that model with front and end wing shows less drag and lift, shows better aerodynamics characteristics than other two models [20].

Jurij Iljaž et al investigated ways to improve a SAE Formula car's rear wing. The primary objective of this work was to demonstrate, through optimization of the rear wing design, the superiority of a slat over a second rear flap in the SAE formula rear wing design, when combined with a 3D curved rear flap, for low velocities. Five distinct main wing height positions and a thorough investigation of the impact of attack angle on wing performance were used to compare the two different main designs. The idea was tested numerically using a 3D shear stress transfer (SST) Reynolds-averaged Navier-Stokes (RANS) simulation that included the entire formula. It was discovered that the multi-element wings were suitable for slow speeds and that the two-flap base design shouldn't be placed too low. The downforce rises with wing height and reaches its maximum at an angle of attack of 8 degrees. This is why the new curved form with a slat and a single flap was suggested. The new wing has a higher lift coefficient, a bigger maximum downforce, and can withstand a greater angle of attack. At the same wing height, the new design produced an increase in downforce of around 6% [21].

Rong Ma et al. conducted research for multi-objective optimization based on S1223 airfoil. Low Reynolds number airfoils that are intended to have a high lift-to-drag ratio at cruising attack angle together with favourable stall characteristics are crucial for the design of a high-performance propeller for low-dynamic aircraft in near space. The paper uses the high-lift airfoil S1223 as the basis for a hierarchical multi-objective optimization, combining the direct search optimization algorithm EXTREM and the airfoil flow field solver XFOIL to quickly and automatically calculate the aerodynamic performance function of the airfoil on a computer. The improved aerofoil S1223 OPT2's aerodynamic performance findings are in line with design specifications. The optimized airfoil that is described here is therefore suggested as the chosen airfoil reference for the high-efficiency propeller of low-dynamic vehicles in the stratosphere [22].

E. Mollica et al investigated the performance of the Low Reynolds S1223 airfoil numerically, using the CFD open-source Open FOAM suite. The sensitivity analysis of the S1223 airfoil's aerodynamic performance over a broad range of Reynolds numbers has been the primary original component of this numerical research. Investigations have focused on the effects at low Reynolds numbers. Reducing the Reynolds has been found to result in a 32% decrease in the maximum lift coefficient. At three different angles of attack ( $4^\circ$ ,  $8^\circ$ , and  $12^\circ$ ), the streams, pressure coefficient distribution, and velocity contour have all been assessed. It can be seen from these representations that when the angle of attack increases, the separation points shift to the left [23].

The front and rear wings of a Formula Student car were described in the study conducted by Abhishek.M.Patil et al, along with its initial design and evolution. The front and rear wings were made to provide the most downforce (negative lift) while staying within the boundaries of permissible drag and top speed increases. This article also covers CFD analysis of front and rear wings and manufacturing. The project's goal was to create an active aerodynamic front package in an effort to improve race vehicle performance. The suggested aerodynamic design includes a wing configuration that enables adjusting the angle of attack. Thermocol and FRP can be used to create strong wings without adding to the vehicle's weight. They arrived at a downforce value of 194.05N after solving [24].

The goal of the study by Andrew R. Hammond et al was to maximize the amount of performance-improving aerodynamic down-force produced by the University of Auckland Formula SAE race car in 2005/2006. This was accomplished utilizing a combination of computational fluid dynamics and physical modelling using a rolling road wind tunnel research facility. The vehicle's body and undercarriage were designed using computational fluid dynamics. A lift coefficient of -0.9 from the under-tray resulted from optimal design. According to simulations, the downforce was boosted by 35% when the exhaust was blown into the two diffuser tunnels underneath the automobile. A lift coefficient of -2.4 was obtained from half-scale vehicle modelling utilizing the wind tunnel rolling road facility. By adjusting the angle of the foils, the aerodynamic load on the front and back wheels, respectively, could be changed from 43% on the front and 57% on the back to 33% on the front and 67% on the back in its ideal configuration. The drag coefficient ranged from 0.9 to 1.1. The experimental strategy was validated by full-scale on-track measurements that revealed just 6% less down-force was produced than was expected by the wind tunnel test program. Data gathered from the car during the endurance event at the 2006 Formula Student Germany competition revealed

that the aerodynamic package was responsible for a notable increase in the performance of the vehicle under braking and during cornering, while the increase in drag force had only a minor impact on the top speed that was achieved during the event [25].

The design, development, and use of an active aerodynamics system on a 2013 Formula SAE car were studied by James Patrick Merkel. The aerodynamics package itself was made up of front and rear wings with five elements each, as well as an underbody diffuser. A compromise between the car's ability to turn and its straight-line acceleration was made by five element wings, which generate a lot of drag. In order to optimize the wings for each situation, the active aerodynamics system enabled the wings' angle of attack to alter dynamically as the vehicle is moving. Computational fluid dynamics is used to analyse the wings in both their maximum lift configuration and their minimum drag configuration. To articulate the wings between these two states, a control system was then constructed employing an electromechanical actuation mechanism [26].

Nisha Rastogi et al conducted a study, where vehicle dynamics and aerodynamics were connected to the point where all the aforementioned criteria could be met, resulting in a trade-off without any form of compromise in either of them. With the aid of a thorough approach and CFD simulations of the car's entire body and the wings using STAR CCM+, the coordination between aerodynamics and vehicle dynamics has been shown. The results have also been appropriately explained in this paper's later sections. The target performance was achieved via a methodical approach, carefully completed with numerous MATLAB iterations, followed by CFD simulations and analysis [27].

Mohammad Arief Dharmawan et al investigated the aerodynamic comparison between a race vehicle with and without wings using 3D computational fluid dynamic simulations. This method of simulation allows for more accurate results than traditional methods, as it takes into account factors such as air pressure, temperature, and velocity in its calculations. The study discusses the aerodynamic comparison between a race vehicle with and without wings, which was studied using 3D computational fluid dynamic simulations. The results showed that attaching wings to the race vehicle decreased its drag coefficient by 23%, and also revealed contour pressure and velocity values [28].

The research by Sven Rehnberg et al was about the design process of an aerodynamic package for a Formula SAE (FSAE) style race car. An aerodynamic package includes components like front wing, rear wing and diffuser which help to reduce drag on the vehicle while driving.

Vehicle data from CFS 2011 FSAE was used during this design phase in order to evaluate how it will affect performance such as lateral/longitudinal acceleration and fuel consumption. Special attention was paid towards post-processing CFD simulations so that valuable insights could be obtained regarding air flow over the vehicle body. The results of this study indicate that although the resolution of CFD simulations was relatively low, valuable insights on how air flows over the vehicle were obtained [29].

The goal of the research by Kyle Sean Lukacovic was to research a new type of rear wing design for Formula SAE cars, which are used in automotive racing. This research consists of three steps: firstly, using computer simulations (CFD) to analyse different configurations; secondly creating an optimal design and building a test rig; finally performing wind tunnel tests on the rig and comparing results with the simulation data. From these results it was concluded that incorporating circulation control wings could significantly improve downforce generated by the wing while reducing drag when not being actively powered - making them beneficial both during acceleration testing as well as races. The main results of this study are that a circulation control device can significantly improve the downforce generated by the wing, and that simulations were validated through physical testing. From these findings it is highly recommended to pursue using such wings in their future cars as they provide both increased performance during acceleration tests and races while also reducing drag when not actively powered [30].

A summary of the state of knowledge on a topic is given in a literature review, along with gaps and potential future research areas. There are a few gaps in the numerical analysis of the aerodynamic behaviour of Selig airfoils with numerous elements, according to the mentioned literature studies. Hence, investigation into the use of multi-element Selig airfoils in various combinations is taken into account to find greater aerodynamic performance.

## CHAPTER III

### Methodology

#### 3.1 Airfoil

In this study, the S1223 airfoil was chosen for the simulations. Fig 3.1 displays the profile. The S1223 airfoil has a maximum chord thickness of 23% and a maximum camber of 1% of the chord, which is positioned 20% of the chord from the leading edge. Chord length was taken into account in this work at 500 mm. The ANSYS design modeler imported the S1223 coordinate file to produce the airfoil.

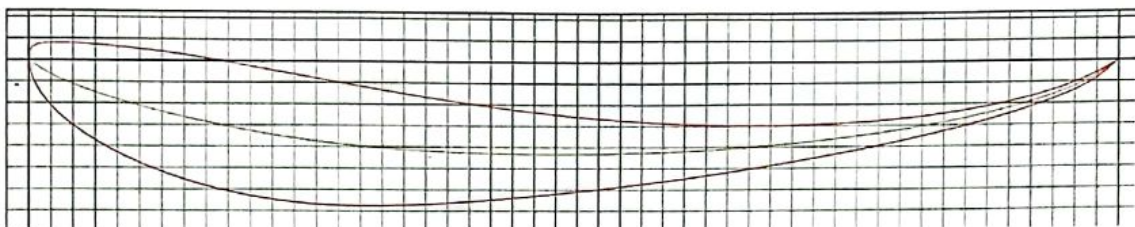


Figure 3. 1 S1223 airfoil's geometry

#### 3.2 CAD Model

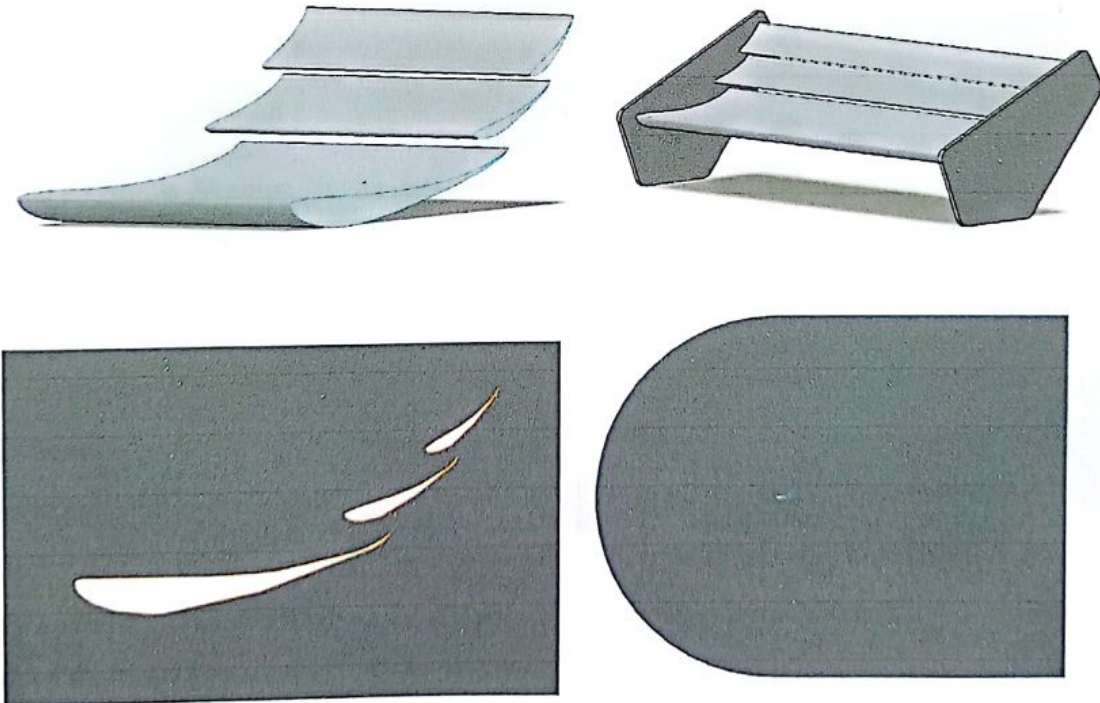


Figure 3. 2 CAD geometry for numerical analysis

CAD modelling was done by using Solidworks, for this analysis 2d surface were needed including airfoil cross section along with the boundary domain. Figure 3.2 illustrates some general CAD geometry essential for this analysis.

### 3.3 Computational Method

ANSYS Fluent was used to carry out these simulations. With the use of two turbulence models, the issue was resolved in steady-state. These simulations were carried out at a fixed Reynolds number ( $Re$ ), which was set at  $3.3 \times 10^5$  to illustrate the influence at the transition area [31]. With  $\rho = 1.225 \text{ kg/m}^3$  and  $\mu = 1.864 \text{ 105 kg/ms}$ , air was taken into account as the working medium.

Calculation of Reynold's number:

$$Re = \frac{\rho VL}{\mu}$$

Air is used for the simulation;

Dynamic viscosity of air  $\mu = 18.6 \times 10^{-6} \text{ Pa s}$ ;

Density of air  $\rho = 1.225 \text{ kg/m}^3$ ;

Air velocity  $V = 10 \text{ m/s}$ ;

and wing chord length  $L$  is approximate 0.5 m

The Reynolds Average Navier-Stokes (RANS) equation was solved using the pressure-based solver and the Green-Gauss cell-based gradient option because the flow was incompressible. The time-averaged equations of motion for fluid flow are known as RANS equations, which are described in below:

$$\frac{\partial(\rho u_i)}{\partial x_i} = 0 \quad (i)$$

$$\frac{\partial(\rho u_i u_j)}{\partial x_j} = \frac{\partial p}{\partial x_i} + \frac{\partial}{\partial x_j} \left[ \mu \left( \frac{\partial u_i}{\partial x_j} + \frac{\partial u_j}{\partial x_i} - \frac{2}{3} \delta_{ij} \frac{\partial u_l}{\partial x_l} \right) \right] + \frac{\partial}{\partial x_j} (-\rho \bar{u}'_i \bar{u}'_j) \quad (ii)$$

here,

$u$  = velocity of the fluid

$\rho$  = density of the fluid

$\mu$  = dynamic viscosity of the fluid

The fluid element's mean momentum shift as a result of flow instability and convection is described on the left side of this equation. The Reynolds stress ( $-\rho \overline{u'_i u'_j}$ ), also known as the mean body force, viscous stresses, isotropic stress resulting from the mean pressure field, and visible stress resulting from the variable velocity field control this adjustment. There are numerous distinct turbulence models as a result of this nonlinear stress term, which necessitates further modelling to solve the RANS equations [32].

The Standard k-model and the SST k-model are both employed in this study to forecast the effects of turbulence on the flow over the airfoil.

## CHAPTER IV

### Numerical Modelling

#### 4.1 Governing Equations

These are the governing equations for steady and 2D incompressible flow:

$$\frac{\partial(\rho u)}{\partial x} + \frac{\partial(\rho v)}{\partial y} = 0 \quad (iii)$$

$$u \frac{\partial(\rho u)}{\partial x} + v \frac{\partial(\rho u)}{\partial y} = - \frac{\partial P}{\partial x} + \frac{\partial \tau_{xx}}{\partial x} + \frac{\partial \tau_{yx}}{\partial y} \quad (iv)$$

$$u \frac{\partial(\rho v)}{\partial x} + v \frac{\partial(\rho v)}{\partial y} = - \frac{\partial P}{\partial y} + \frac{\partial \tau_{xy}}{\partial x} + \frac{\partial \tau_{yy}}{\partial y} \quad (v)$$

$$\rho c_v \frac{dT}{dt} = k \nabla^2 T + \phi \quad (vi)$$

here,

$$\tau_{xx} = 2\mu \frac{\partial u}{\partial x},$$

$$\tau_{yy} = 2\mu \frac{\partial v}{\partial y}$$

$$\tau_{xy} = \tau_{yx} = \mu \left( \frac{\partial u}{\partial y} + \frac{\partial v}{\partial x} \right)$$

$$\phi = \mu [2 \left( \frac{\partial u}{\partial x} \right)^2 + 2 \left( \frac{\partial v}{\partial y} \right)^2 + (\frac{\partial u}{\partial y} + \frac{\partial v}{\partial x})^2]$$

Equation (iii) represents continuity equation, equation (iv) and (v) represents Navier-Stokes; and equation (vi) deals with energy.  $u$  is the velocity in the  $x$ - and  $y$ -direction,  $v$  is the velocity in the  $y$ -direction,  $\mu$  is the viscosity,  $\rho$  is the density,  $P$  is the pressure,  $\tau$  is the shear stress,  $\phi$  is the viscous dissipation function, and  $T$  is the temperature.

## 4.2 SST k- $\omega$ Model

The SST stands for Menter's Shear Stress Transport turbulence model. The SST k- $\omega$  model is a commonly utilized turbulence model with two equations for eddy viscosity in computational fluid dynamics (CFD) analysis. Menter created this model by combining the near-wall precision and robustness of the k- $\omega$  model with the free-stream independence of the k- $\epsilon$  model in the far field. This was achieved by transforming the k- $\epsilon$  model into a k- $\omega$  formula. The SST k- $\omega$  model is similar to the standard k- $\omega$  model but includes several enhancements:

- i. The k- $\omega$  standard model and the modified k- $\epsilon$  model are integrated and merged using a blending function. This function is created to be equal to one in the vicinity where the k- $\omega$  model is employed and drops to zero where the modified k- $\epsilon$  model is applied.
- ii. The omega equation of the SST model includes a damp cross-cutting factor.
- iii. In addition, by expressing the turbulent shear stress, the turbulent viscosities are better described.
- iv. Numerous modelling constants are available.

The following transport equations are used to calculate the turbulent kinetic energy, k, and the eddy viscosity dissipation rate,  $\omega$ :

$$\frac{\partial(\rho k)}{\partial t} + \frac{\partial(\rho k u_i)}{\partial x_i} = \frac{\partial}{\partial x_j} \left( \Gamma_k \frac{\partial k}{\partial x_j} \right) + G_k - Y_k + S_k \quad (vii)$$

$$\frac{\partial(\rho \omega)}{\partial t} + \frac{\partial(\rho \omega u_i)}{\partial x_i} = \frac{\partial}{\partial x_j} \left( \Gamma_\omega \frac{\partial \omega}{\partial x_j} \right) + G_\omega - Y_\omega + D_\omega + S_\omega \quad (viii)$$

These equations involve  $G_k$ , which represents the creation of turbulence kinetic energy from mean velocity changes, and  $G_\omega$ , which stands for the creation of  $\omega$ . The effectiveness of diffusing k and  $\omega$  is shown by  $\Gamma_k$  and  $\Gamma_\omega$ , which can be computed using the methods described. Turbulence causes the decay of k and  $\omega$ , represented by  $Y_k$  and  $Y_\omega$ . The cross-diffusion term,  $D_\omega$ , can be calculated according to the instructions provided.  $S_k$  and  $S_\omega$  are sources that the user can define.

$$\Gamma_k = \mu + \frac{\mu_t}{\sigma_k}$$

$$\Gamma_\omega = \mu + \frac{\mu_t}{\sigma_\omega}$$

The turbulent Prandtl numbers for  $k$  and  $\omega$  are denoted by  $\sigma_k$  and  $\sigma_\omega$  respectively. The turbulent viscosity, represented by  $\mu_t$ , can be computed using the following formula.

$$\mu_t = \frac{\rho k}{\omega} \frac{1}{\max\left[\frac{1}{\alpha^*}, \frac{SF_2}{a_1 \omega}\right]}$$

where,  $S$  stands for strain rate magnitude,  $\alpha$  for attack angle, and

$$\sigma_k = \frac{1}{F_1/\sigma_{k,1} + (1-F_1)/\sigma_{k,2}},$$

$$\sigma_\omega = \frac{1}{F_1/\sigma_{\omega,1} + (1-F_1)/\sigma_{\omega,2}} \text{ and } F_1, F_2 \text{ are the blending functions.}$$

### 4.3 Computational Domain and Boundary Conditions

To conduct simulations, a computation domain was established around the S1223 airfoil, similar as depicted in Figure 4.1. The chord length of the airfoil was assumed to be 500 mm. To minimize boundary effects, the domain was extended 12.5 times the chord length upstream and 20 times the chord length downstream from the trailing edge, as shown in Figure 4.1 [33]. The airfoil surface was assumed to have a no-slip boundary condition, while a constant velocity inlet (BAFED) and pressure outlet (BCD) were utilized. A fixed Re value was used, with an assumed inlet velocity of 10 m/s. Instead of rotating the airfoil, the angle of attack ( $\alpha$ ) was modified by altering the flow direction, which had the same impact on the airfoil. The  $x$  and  $y$  velocity components were determined by calculating  $(u \cos \alpha)$  and  $(-u \sin \alpha)$  (for inverted geometry), respectively, for various angles of attack ( $\alpha$ ).

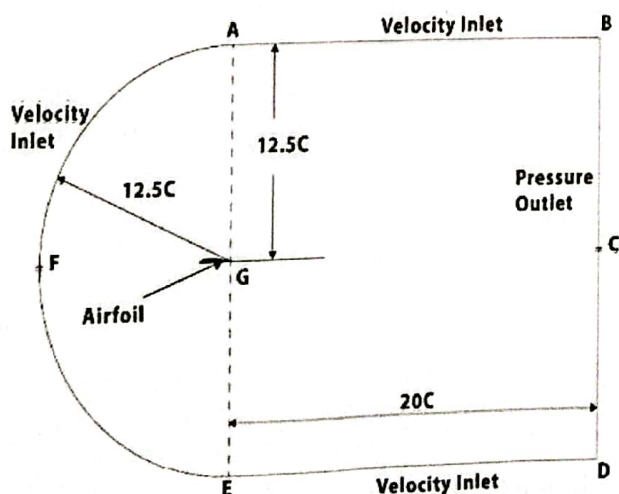


Figure 4.1 Computation domain with boundary conditions

#### 4.4 Mesh Generation for Baseline Airfoil

To enhance the accuracy and management of the wall function, the C-type structural mesh was developed and illustrated in Fig. 4.2 and Fig. 4.3. ANSYS Meshing was employed to create the quadrilateral elements in the structural mesh displayed in Fig. 4.2, while the meshing quality surrounding the airfoil profile is portrayed in Fig. 4.3.

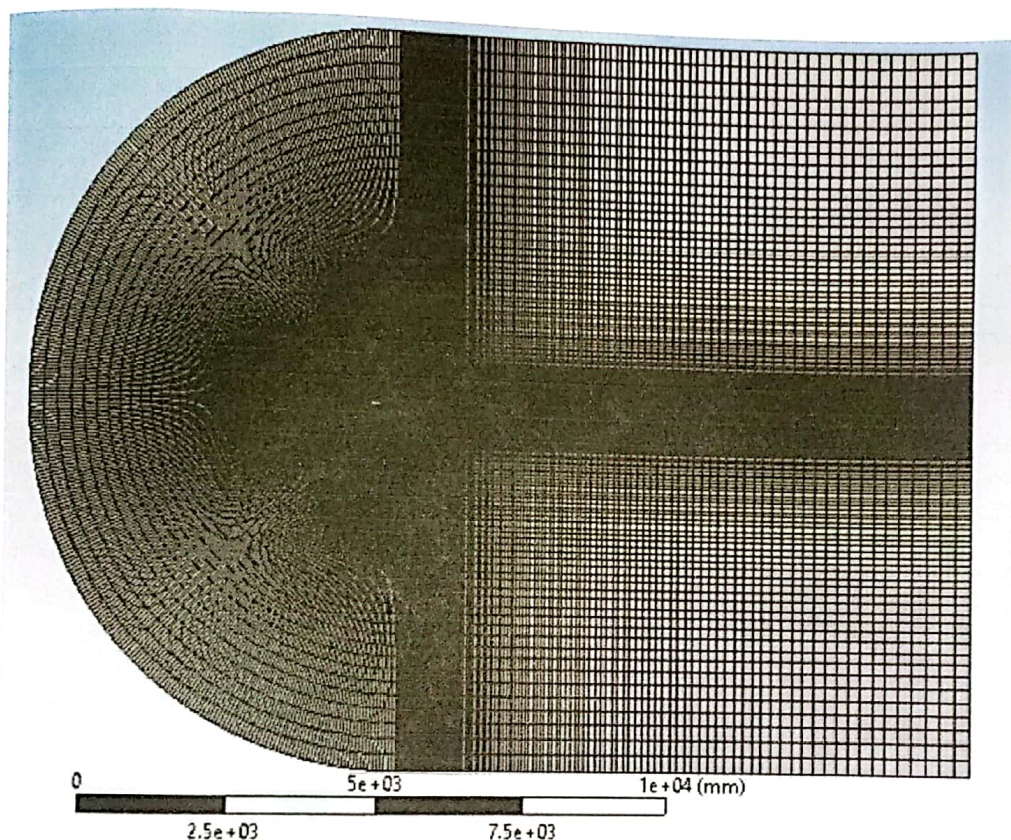


Figure 4. 2 Mesh inside the entire domain

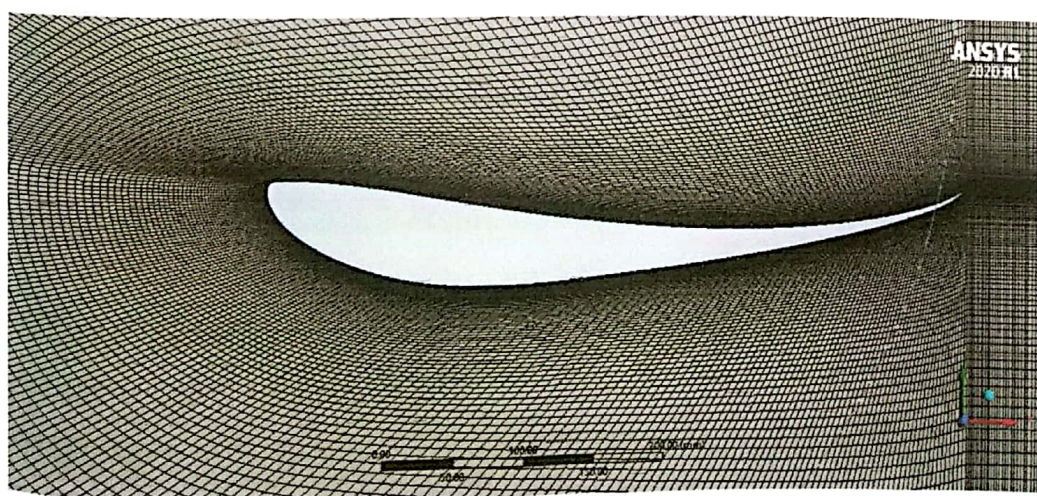


Figure 4. 3 Mesh around the S1223 airfoil

#### 4.5 Mesh Independence Test for Baseline airfoil

Mesh independence tests were carried out using a number of simulations. Fig. 4.4 shows the change in negative lift coefficient for various mesh element counts at a  $5^\circ$  angle of attack. The figure shows that meshes with more than 105000 pieces can yield precise results with little variation. The mesh with element number 105000 was therefore chosen for additional simulation.

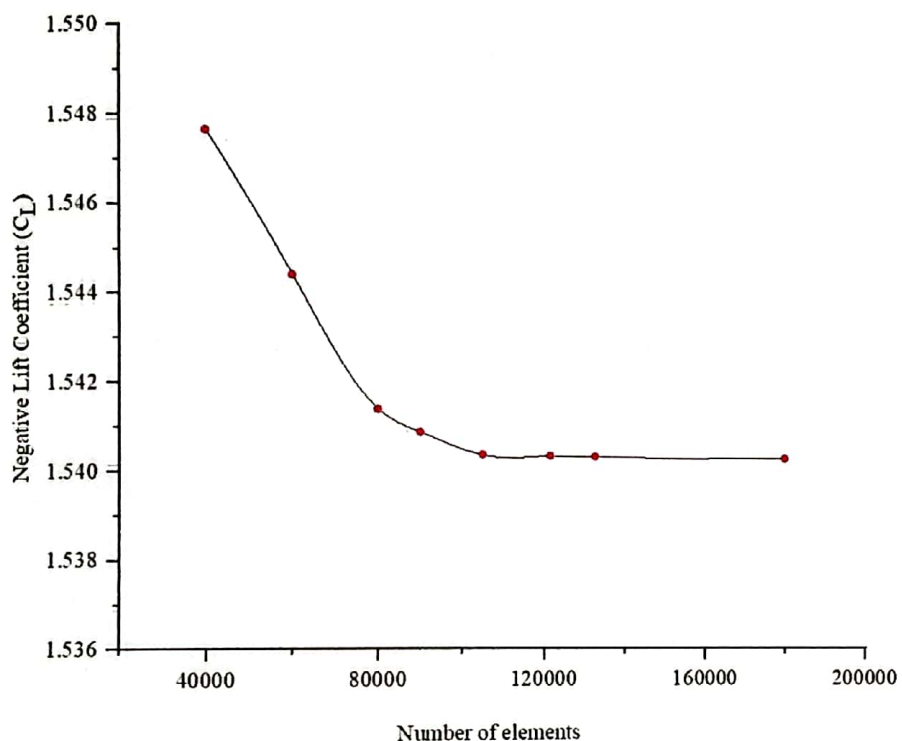


Figure 4. 4 Variation of negative lift coefficient with number of elements

#### 4.6 Mesh Generation for Multi-Element Airfoil cross section

The multi-element mesh is depicted in Fig. 4.5 and 4.6. Fluent meshing was used for the meshing. An extremely tiny mesh setting was chosen for the mesh generation. Additionally, an inflation layer was included to capture the impacts of the border layer. In settings, 20 inflation layers were added, with a skewness ratio of 0.0785, the rear wing's aspect ratio was 3.3956. Orthogonality was 0.9578 at the time. These fall within the parameters of what ANSYS Fluent considers to be a good mesh. The different meshing parameters are listed together with their matching values in Table 4.1.

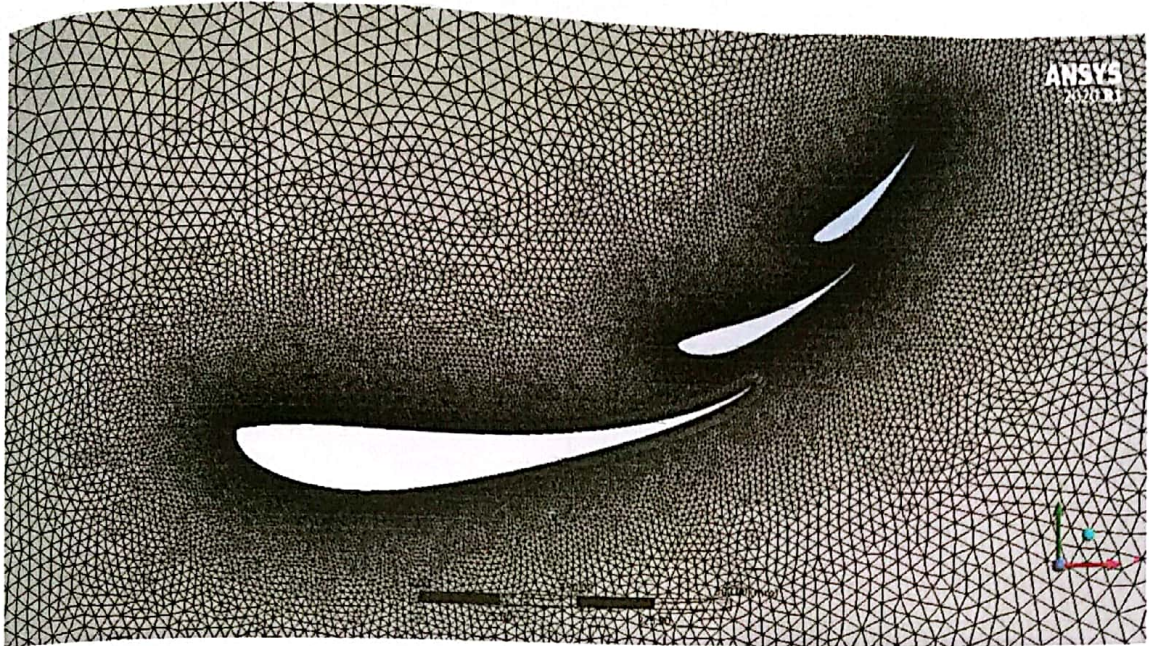


Figure 4. 5 Meshing for multi-element airfoil cross section

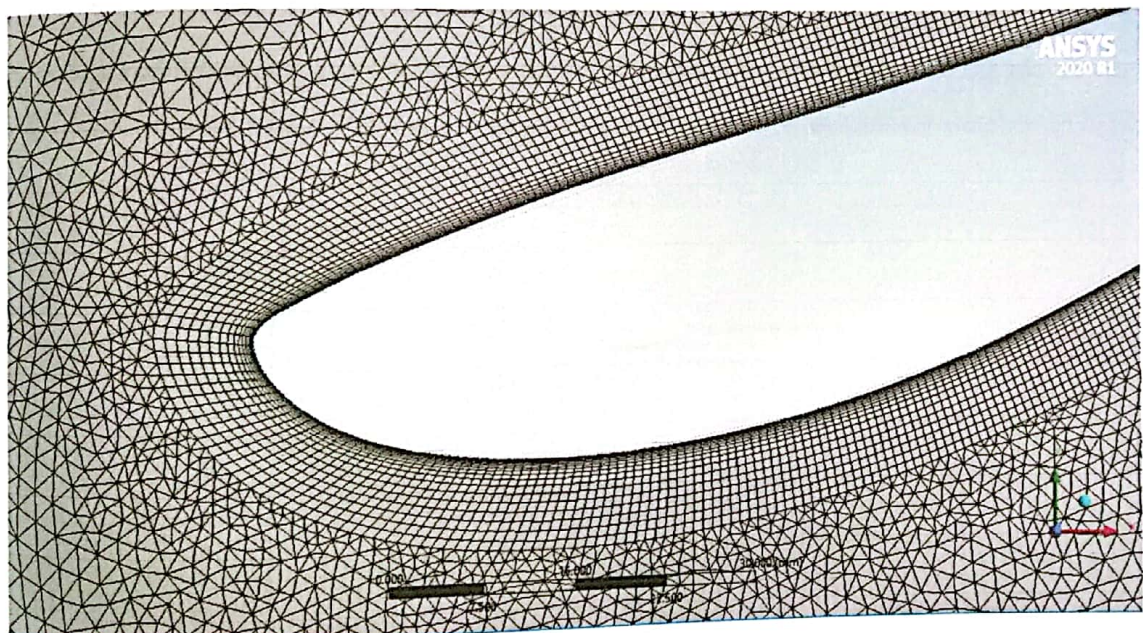


Figure 4. 6 Detailed view of mesh for r multi-element airfoil cross section with inflation layer

Table 4. 1 Meshing parameters

Parameter	Value / Condition
Mesh size	Fine mesh
Number of Inflation Layers	20
Aspect Ratio	3.3956
Skewness	0.0785
Orthogonal quality	0.9578

#### 4.7 Mesh Independence Test for Multi-element Airfoil cross section

The Airfoils cross section geometries with different chord lengths (500 mm, 200 mm and 150 mm) and decorated in a set of angles of attack in the order  $8^\circ$ ,  $28^\circ$ ,  $46^\circ$  was chosen for mesh independence test. Fig. 4.7 shows how the negative lift coefficient varies depending on how many mesh elements are present. It showed that meshes with more than 142552 pieces can yield precise results with a low degree of variation. The mesh with element number 142552 was consequently chosen for additional simulation.

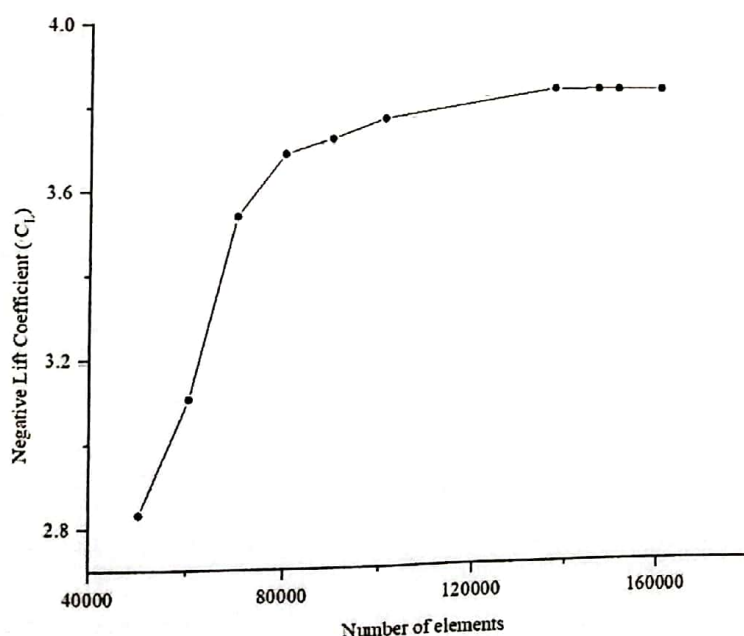


Figure 4. 7 Variation of negative lift coefficient with number of elements

#### 4.8 Numerical Set-up

The numerical issue in the current study is resolved using ANSYS Fluent utilizing a Pressure-based solver. Table 4.2 provides a list of the numerical configuration

Table 4. 2 Numerical Setup and Solver Settings

Parameter	Setup/Value
Solver Type	Pressure-Based
Velocity Formulation	Absolute
Time	Steady
2D Space	Planar
Gravity	Off
Multiphase	Off
Energy	Off
Viscous Model	Viscous (SST k- $\omega$ )
Radiation	Off
Fluid	Air
Density	Ideal-Gas
Viscosity (kg/m-s)	Constant, 1.7894e-05

Following Table 4.3 is a collection of the several solution methods for this setup:

Table 4. 3 Solution Methods

Parameter	Setup/Value
Scheme	Coupled
Gradient	Least Square Cell Based
Pressure	Second Order
Momentum	Second Order Upwind
Turbulent Kinetic Energy	Second Order Upwind
Specific Dissipation Rate	First Order Upwind

Table 4.4 displays the solution controls:

Table 4.4 Solution controls

Parameter	Setup/Value
Pressure	0.5
Momentum	0.5
Turbulent Kinetic Energy	0.75
Specific Dissipation	0.75
Turbulent Viscosity	1

#### 4.9 Validation

In this study, the alterations in negative lift coefficient ( $C_L$ ) in relation to the angle of attack ( $\alpha$ ) were compared to the findings of Ali Doosttalab et al. [34]. Their objective was to examine and evaluate the aerodynamic characteristics of damaged low-Reynolds and high-lift UAV airfoils, utilizing two-dimensional numerical simulations under low Reynolds number flow conditions. The outcomes obtained through numerical analysis in the present study correspond well with those of Ali Doosttalab et al. [34].

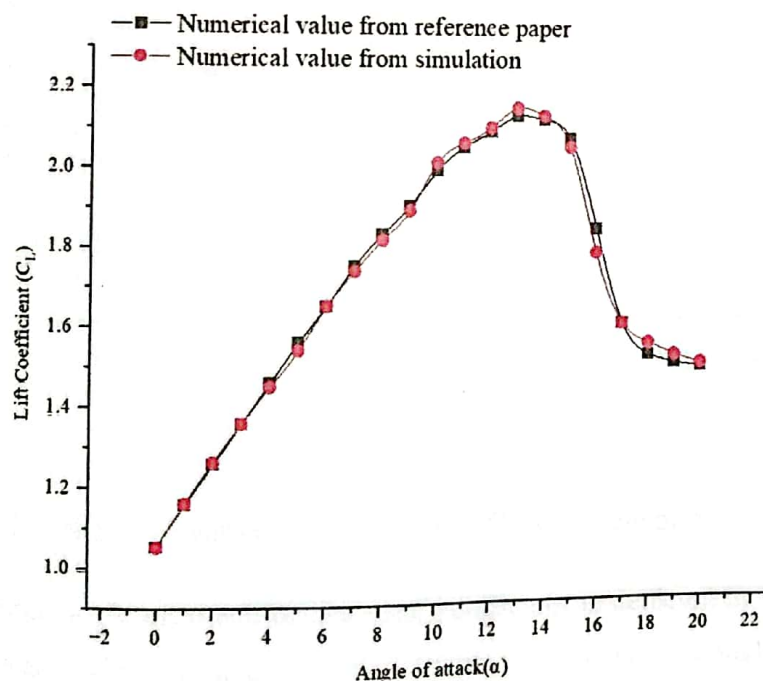


Figure 4.8 Comparison between the variation of  $C_L$  Vs  $\alpha$  with the result of Ali Doosttalab et al. [34]

## CHAPTER V

### Results and Discussion

#### 5.1 Changes of Negative Lift Coefficient and Drag Coefficient for baseline airfoil

Fig. 5.1 shows how the negative lift coefficient varies depending on the angle of attack. It demonstrates that the negative lift coefficient rises with angle of attack, reaching a maximum of  $13^\circ$ . Later, it starts to fall off with because of the flow separation at the trailing edge, which showed that stalling happens between  $13^\circ$  and  $14^\circ$ .

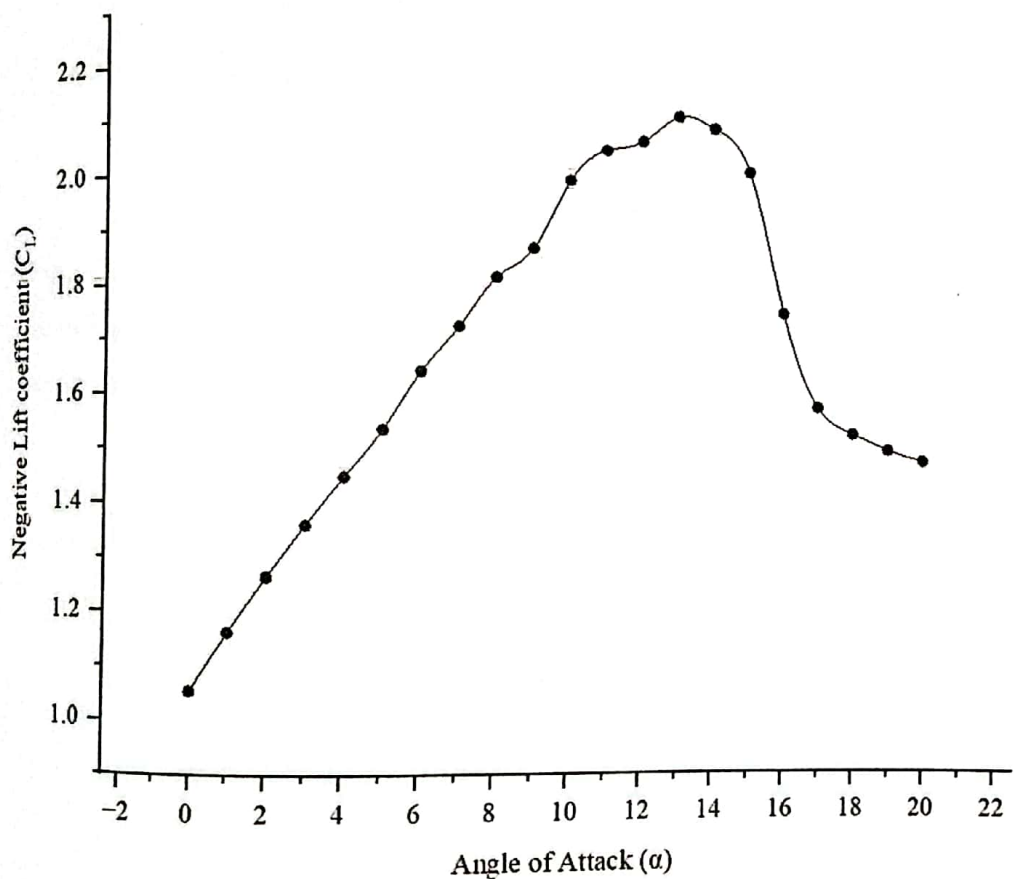


Figure 5. 1 Negative Lift coefficient ( $C_L$ )Vs Angle of Attack ( $\alpha$ )

The impact of the angle of attack on the drag coefficient is depicted in Fig. 5.2. The drag coefficient increases with, although the increment rate is faster at higher angle of attack because of flow separation at the trailing edge. Following the stalling angle, the drag coefficient still rises while the negative lift coefficient falls.

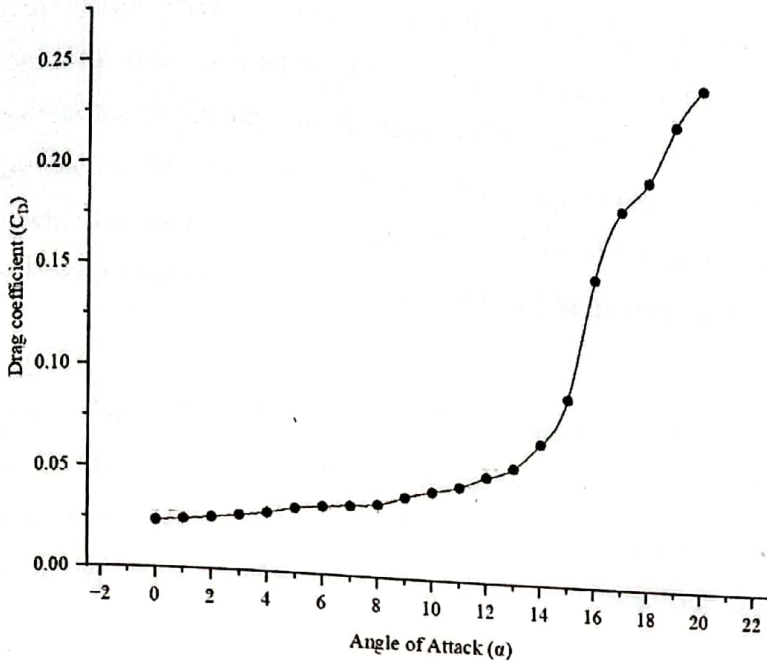


Figure 5. 2 Drag coefficient ( $C_D$ ) Vs Angle of Attack ( $\alpha$ )

The effect of the angle of attack on the ratio of  $C_L/C_D$  also known as lift to drag ratio is displayed in Fig. 5.3. It is observed that the ratio is at peak for the angle of attack 8 degree. The value rapidly falls after this point.

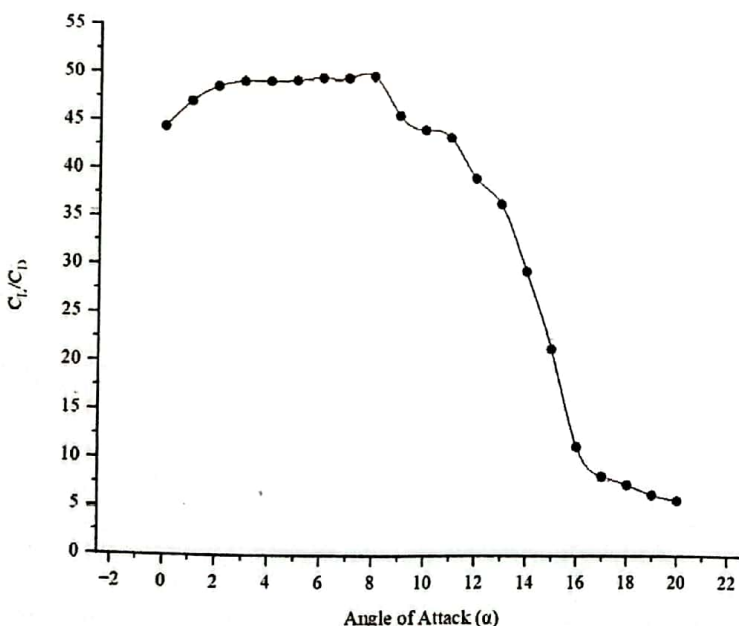


Figure 5. 3 ( $C_L/C_D$ ) Vs Angle of Attack ( $\alpha$ )

There are several reasons why the  $C_L/C_D$  ratio falls after a certain angle of attack in an airfoil. One important reason is the separation of the airflow from the airfoil's surface. As the angle of

attack increases, the airflow over the top surface of the airfoil begins to separate, causing the formation of a turbulent wake behind the airfoil. This separation of the airflow reduces the pressure difference between the top and bottom surfaces of the airfoil, which reduces the negative lift generated by the airfoil and increases the drag. Another reason is the boundary layer separation, which is when the airflow near the surface of the airfoil separates due to a change in the airflow's direction. This separation results in an increase in drag and a decrease in lift.

In summary, the  $C_L/C_D$  ratio falls after a certain angle of attack in an airfoil due to the separation of the airflow from the airfoil's surface, which reduces the lift generated by the airfoil, and the boundary layer separation, which increases the drag. These phenomena are collectively known as stall, and it is an important consideration in designing and analysing the performance of airfoils.

Variation of negative lift and drag force with respect to angle of attack is displayed in figure 5.4 and 5.5 respectively. It is observed that negative lift gradually increases for up to  $13^\circ$ . Then stalling occurs and the value of negative lift rapidly fall. However, drag increases as the angle of attack increases.

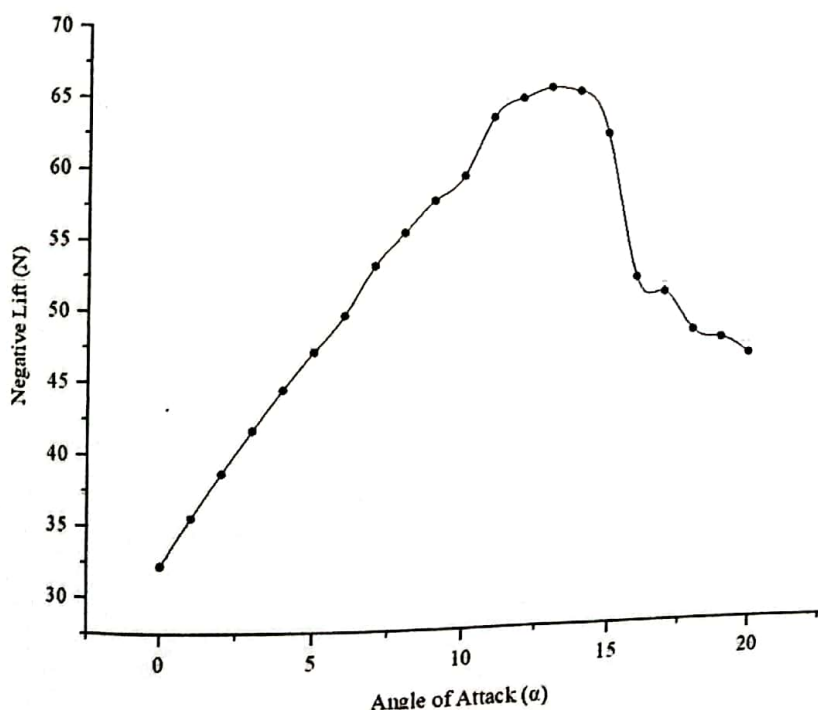


Figure 5.4 Negative lift vs angle of attack

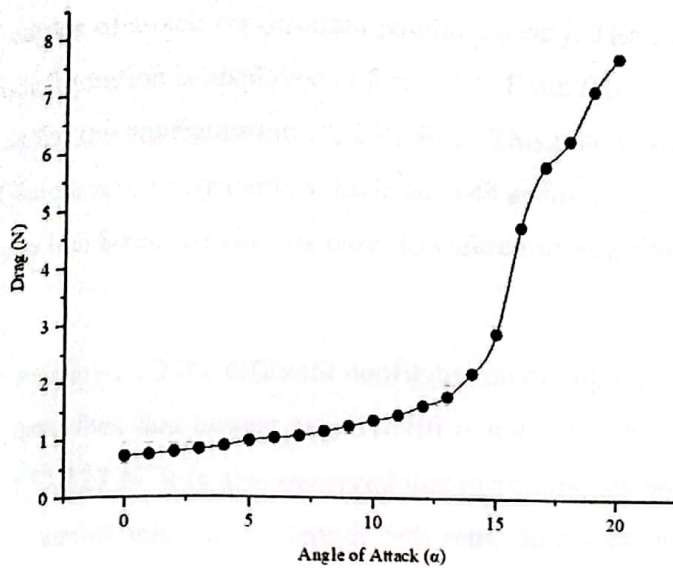


Figure 5. 5 Drag vs angle of attack

### Analysis of multi-element airfoil cross section

has been noted that the most favourable aerodynamic characteristics can be achieved through various parameters, including the ratio of  $C_L/C_D$ , negative lift, negative lift coefficient, drag, and drag coefficient.

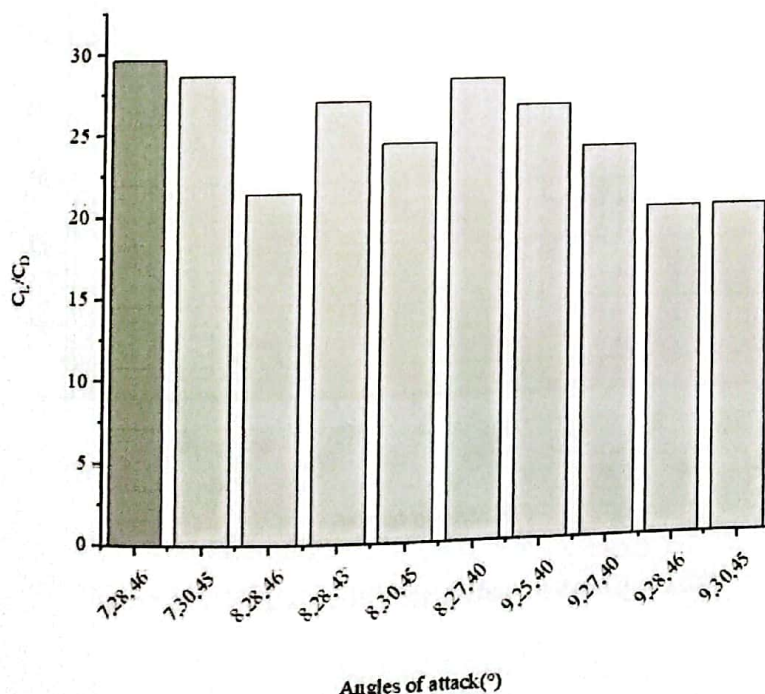


Figure 5. 6 The ratio of  $C_L / C_D$  for different sets of angles of attack (Degree)

The optimal sets of angles of attack for different conditions vary. The variation of the ratio of  $C_L/C_D$  for different configuration is displayed at figure 5.6. From figure, it is observed that the ratio  $C_L/C_D$  is largest for the configuration  $7^\circ, 28^\circ, 46^\circ$ . This ratio is an important parameter to determine how efficient an aerodynamic vehicle is, such as for a larger value of  $C_L/C_D$  it is considered the vehicle has large lift (in this case downforce or negative lift) and small drag which is desirable.

The variation of the negative lift for different configuration of angle of attack is displayed at figure 5.7. The plot describes that largest negative lift is found for the configuration  $8^\circ, 28^\circ, 6^\circ$ , with a value of 153.127 N. It is also observed that increasing the angle of attack from  $8^\circ$  to  $9^\circ$ , for the largest airfoil with chord length 500 mm, decreases the negative lift. Also decreasing the angle of attack from  $8^\circ$  to  $7^\circ$  slightly decreases the negative lift from 153.127 N to 151.2992 N.

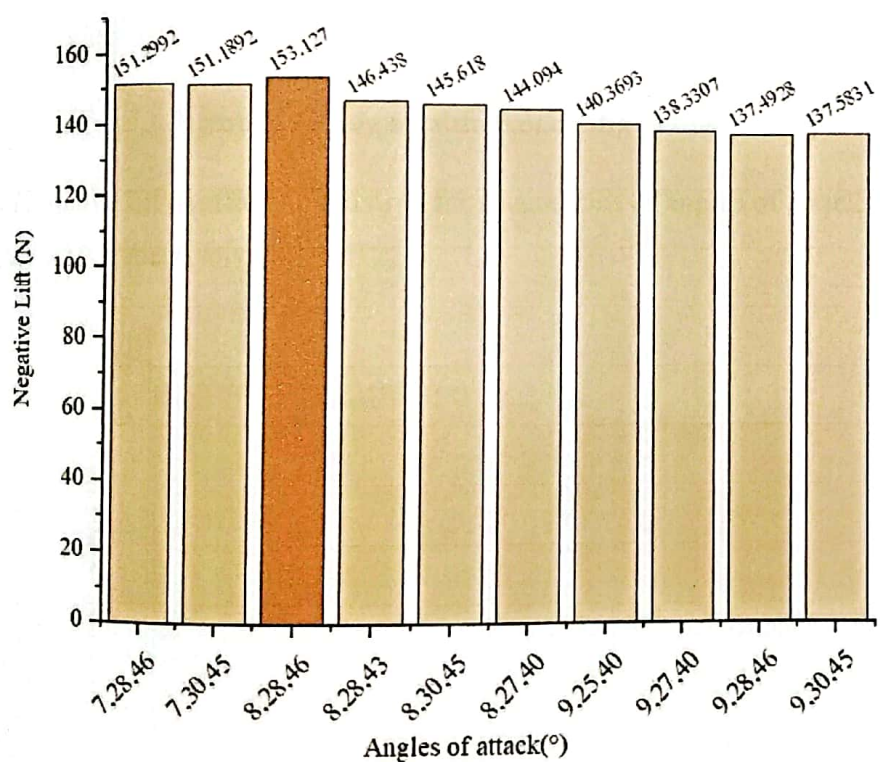


Figure 5. 7 Negative lift for different configuration

The variation of the Drag for different configuration of angle of attack is displayed at figure 5.8. The plot describes that lowest drag is found for the configuration  $8^\circ$ ,  $27^\circ$ ,  $40^\circ$ , with a value of  $5.0959$  N.

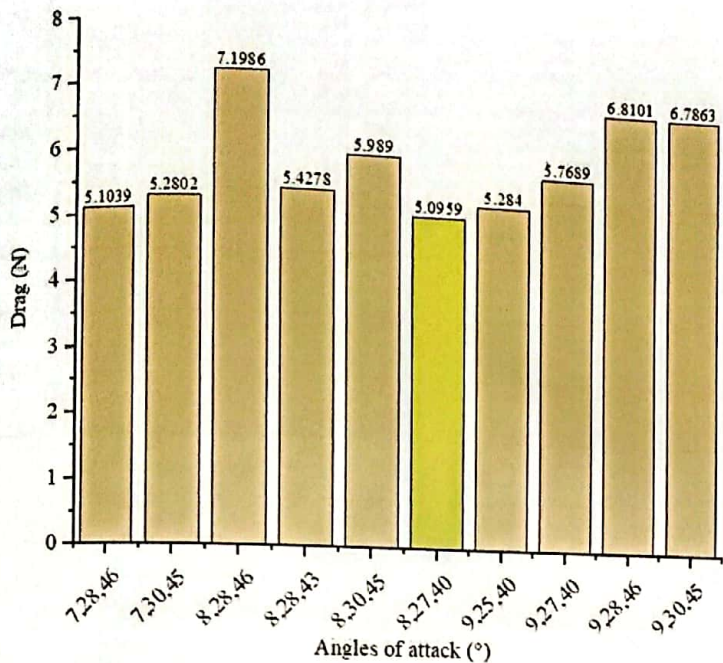


Figure 5. 8 Drag for different configuration

Variation of negative lift coefficient and drag for several sets of angles of attack is shown in figure 5.9 and 5.10 respectively.

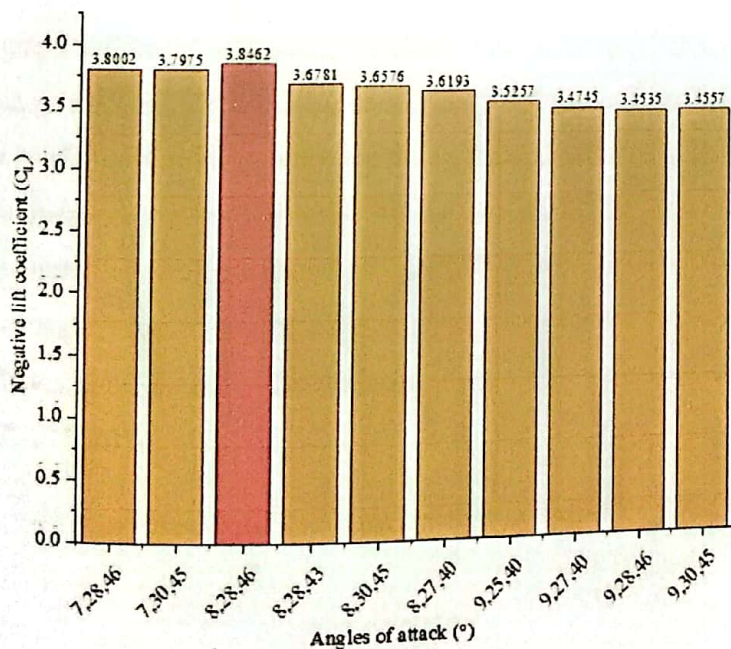


Figure 5. 9  $C_L$  for different configuration

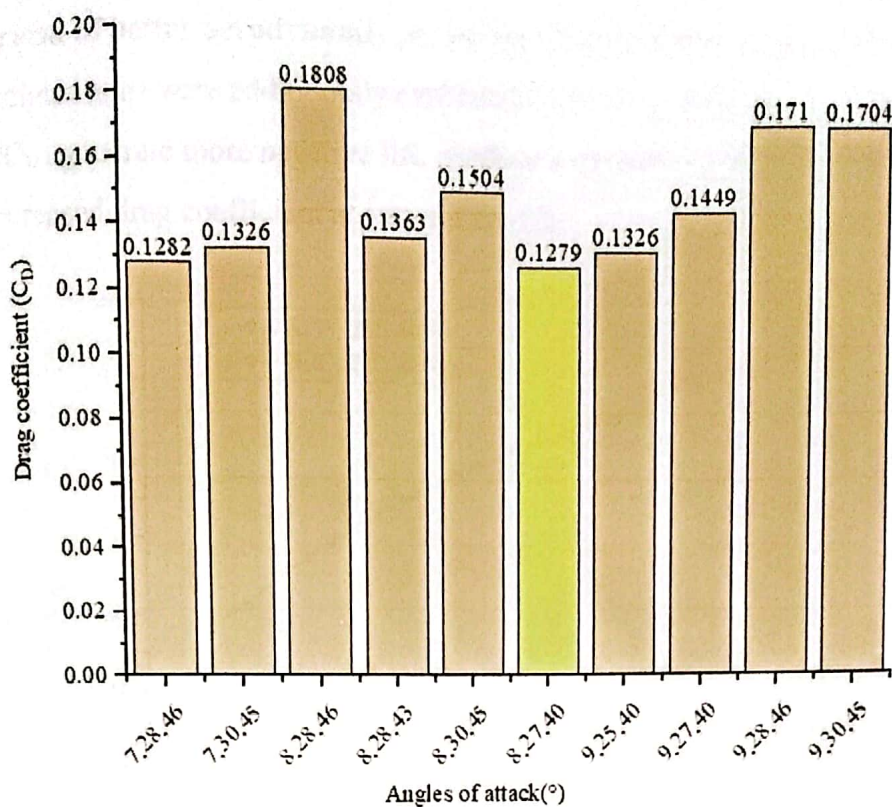


Figure 5. 10  $C_D$  for different configuration

It is observed that highest negative lift coefficient,  $C_L$  is obtained for the configuration of  $8^\circ$ ,  $28^\circ$ ,  $46^\circ$ . Which means impact of the separation of the airflow is less effective in this configuration. Again, the lowest drag coefficient,  $C_D$  is obtained in the configuration of  $8^\circ$ ,  $27^\circ$ ,  $40^\circ$ .

According to the graph and bar charts, there are three different sets of angles of attack that have better aerodynamic properties. The optimal configuration for the highest  $C_L/C_D$  ratio is A( $7^\circ$ ,  $28^\circ$ ,  $46^\circ$ ), the best configuration for generating the highest amount of negative lift is B( $8^\circ$ ,  $28^\circ$ ,  $46^\circ$ ), and the configuration that exhibits the lowest drag is C( $8^\circ$ ,  $27^\circ$ ,  $40^\circ$ ). However, even though the drag generated by configuration C( $8^\circ$ ,  $27^\circ$ ,  $40^\circ$ ) is the lowest, the amount of negative lift it generates is significantly less than the other two configurations. Therefore, when comparing the different configurations for their aerodynamic properties, it was decided to avoid configuration C( $8^\circ$ ,  $27^\circ$ ,  $40^\circ$ ).

### 5.3 Comparison of better aerodynamic properties between two configurations

The two configurations were additionally evaluated in terms of their ability to achieve a higher ratio of  $C_L/C_D$ , generate more negative lift, produce a greater negative lift coefficient, reduce drag, and decreased drag coefficient at varying speeds.

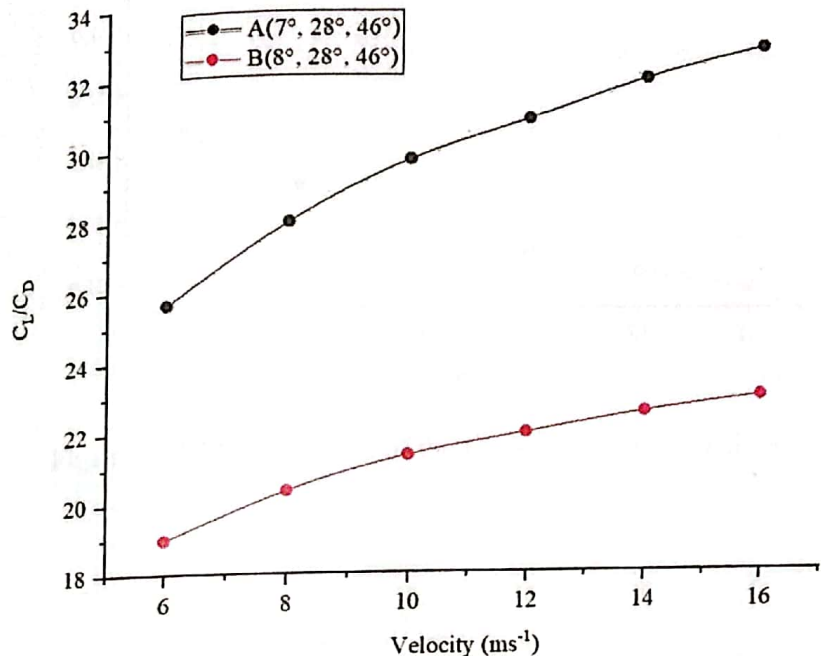


Figure 5. 11 Comparison of the  $C_L/C_D$  ratio for different velocities

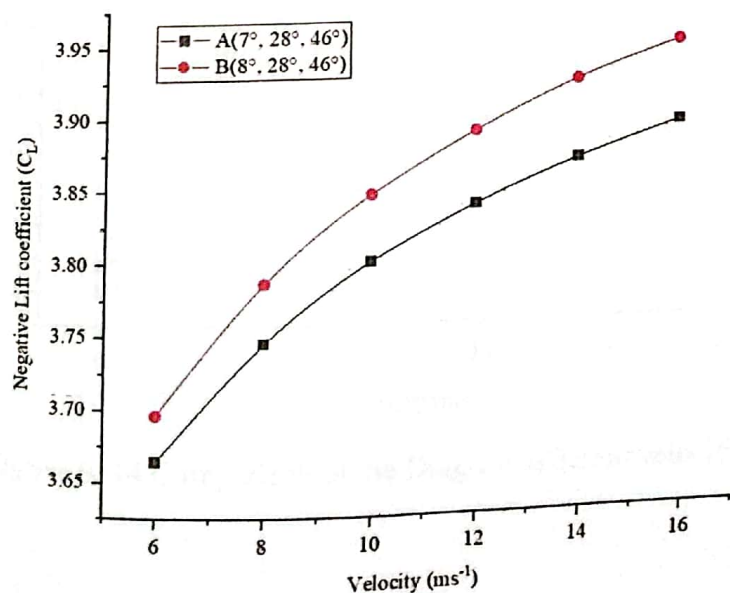
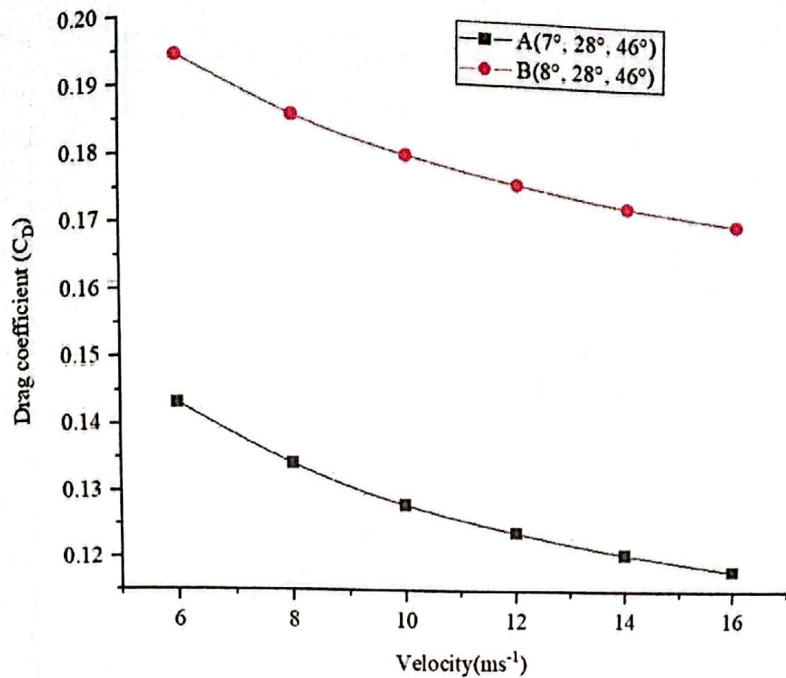
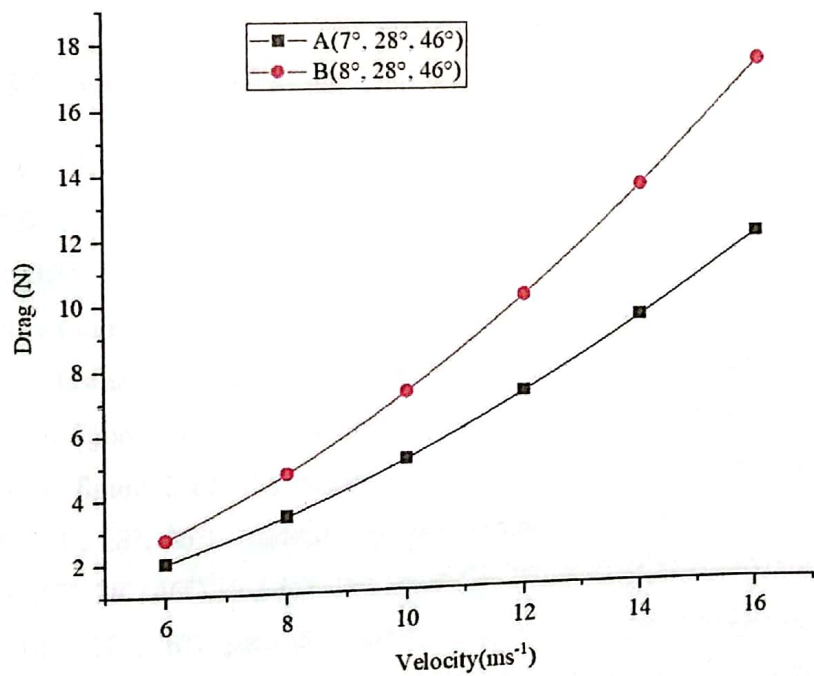


Figure 5. 12 Comparison of the  $C_L$  for different velocities



**Figure 5. 13** Comparison of the  $C_D$  for different velocities



**Figure 5. 14** Comparison of the Drag for different velocities

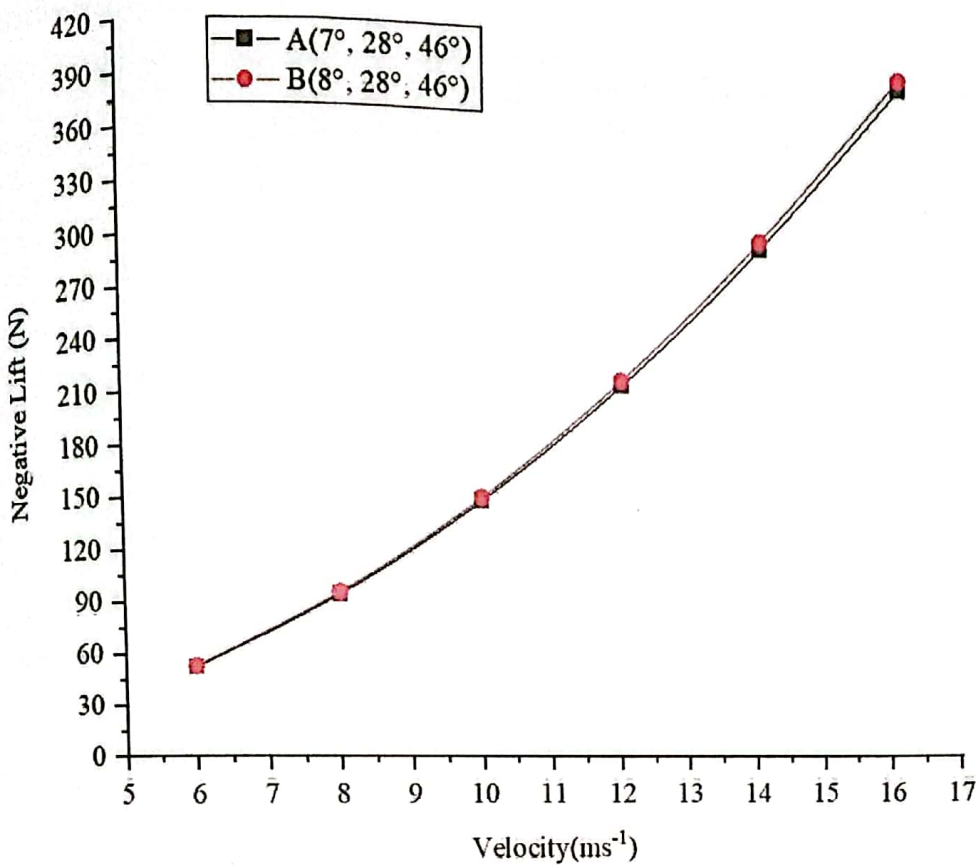


**Figure 5. 15** Comparison of the negative lift for different velocities for different velocities

Based on figure 5.15, it can be observed that both configuration A( $7^\circ, 28^\circ, 46^\circ$ ) and configuration B( $8^\circ, 28^\circ, 46^\circ$ ) result in negative lift with only a slight difference between them. Configuration B( $8^\circ, 28^\circ, 46^\circ$ ) generates slightly more lift than configuration A( $7^\circ, 28^\circ, 46^\circ$ ). However, when examining other graphs, it becomes evident that configuration A( $7^\circ, 28^\circ, 46^\circ$ ) has significantly lower drag than configuration B( $8^\circ, 28^\circ, 46^\circ$ ) at different velocities, as seen in figure 5.14. In figure 5.13, drag coefficients are much smaller in configuration A( $7^\circ, 28^\circ, 46^\circ$ ), while in figure 5.12, the negative lift coefficients are only marginally larger in configuration B( $8^\circ, 28^\circ, 46^\circ$ ). Additionally, the crucial  $C_L/C_D$  ratio is moderately higher in configuration A( $7^\circ, 28^\circ, 46^\circ$ ) for different velocities. Thus, it can be concluded that, although configuration B( $8^\circ, 28^\circ, 46^\circ$ ) generates slightly higher negative lift, considering all the factors, configuration A( $7^\circ, 28^\circ, 46^\circ$ ) is better suited for generating slightly less negative lift with a much higher  $C_L/C_D$  ratio and much lower drag. Therefore, configuration A( $7^\circ, 28^\circ, 46^\circ$ ) can be considered to have overall better aerodynamic properties.

#### 5.4 Velocity contours:

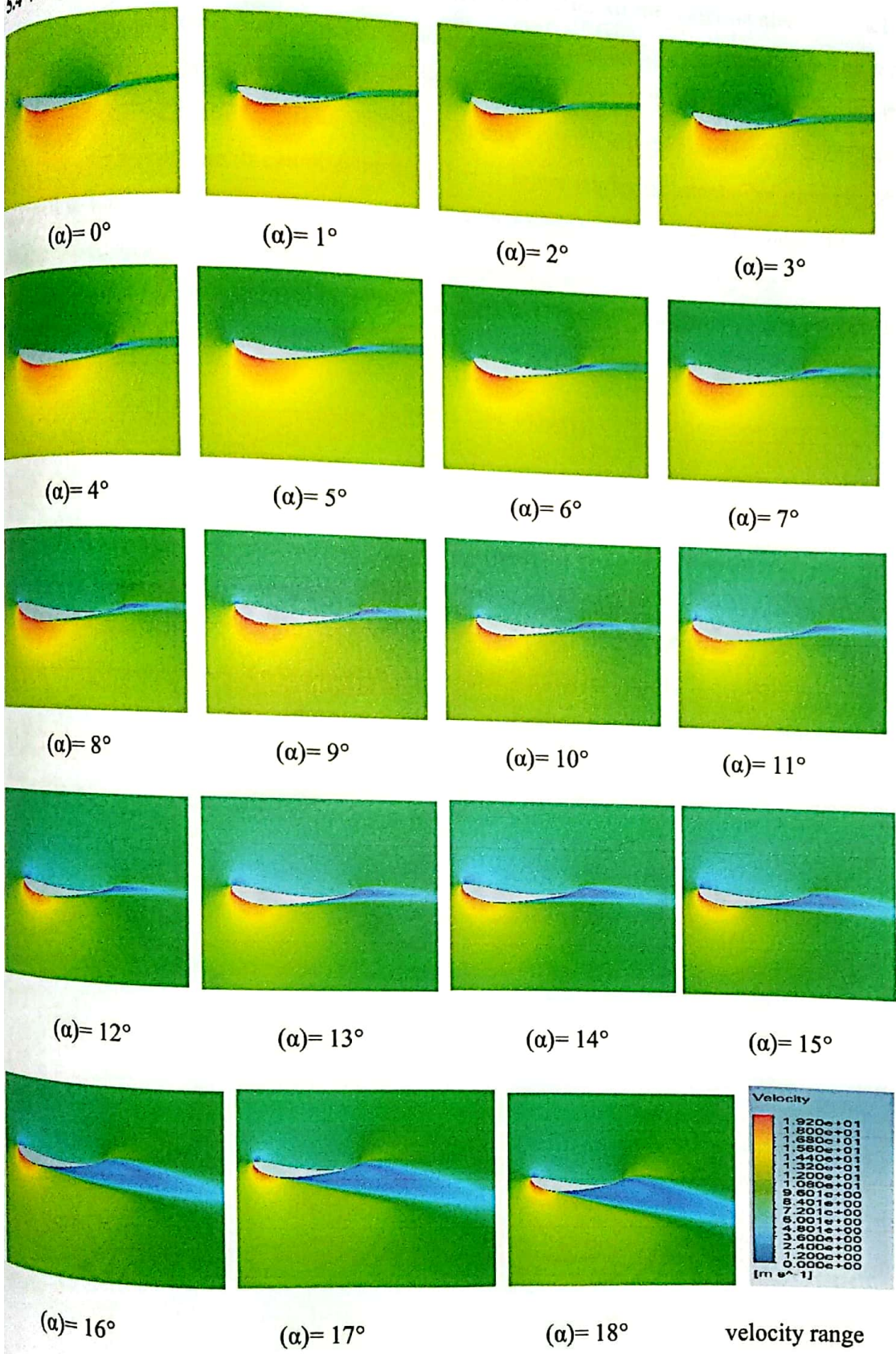


**Figure 5. 16** Baseline airfoil's velocity contours for various angles of attack ( $\alpha$ )

The diagrams in Figure 5.16 illustrate the velocity distribution of the baseline airfoil model at different angles of attack. Rather than physically rotating the airfoil, the flow direction was changed to simulate the same effect. These diagrams clearly show that the velocity below the lower surface of the airfoil is greater than the velocity above the upper surface, in accordance with Bernoulli's principle. It can also be seen that at lower angles of attack, the flow remains attached to both the upper and lower surfaces, with no area of zero velocity indicating flow separation. At an angle of attack of  $13^\circ$ , flow separation begins at the trailing edges and moves towards the leading edges at higher angles of attack. As a result of this flow separation, the lift coefficient starts to decrease beyond a certain angle of attack.

Bernoulli's principle is a fundamental concept that explains the relationship between fluid velocity and pressure. It states that in a steady flow of an incompressible fluid, an increase in the fluid's velocity occurs simultaneously with a decrease in pressure, and vice versa. This principle is essential in understanding the lift force generated by an airfoil. As the fluid flows over the curved upper surface of an airfoil, it must travel a greater distance than the fluid moving along the flat lower surface. This results in a higher velocity on the upper surface, which in turn generates a lower pressure due to Bernoulli's principle. The higher pressure on the lower surface of the airfoil then produces a net upward force, which is the lift force that allows the aircraft to take off and stay airborne. In this case the lift is negative lift or downforce as the airfoil is oriented in inverse. So the higher velocity is observed below the lower surface of airfoil.

**5.5 Pressure contours:**

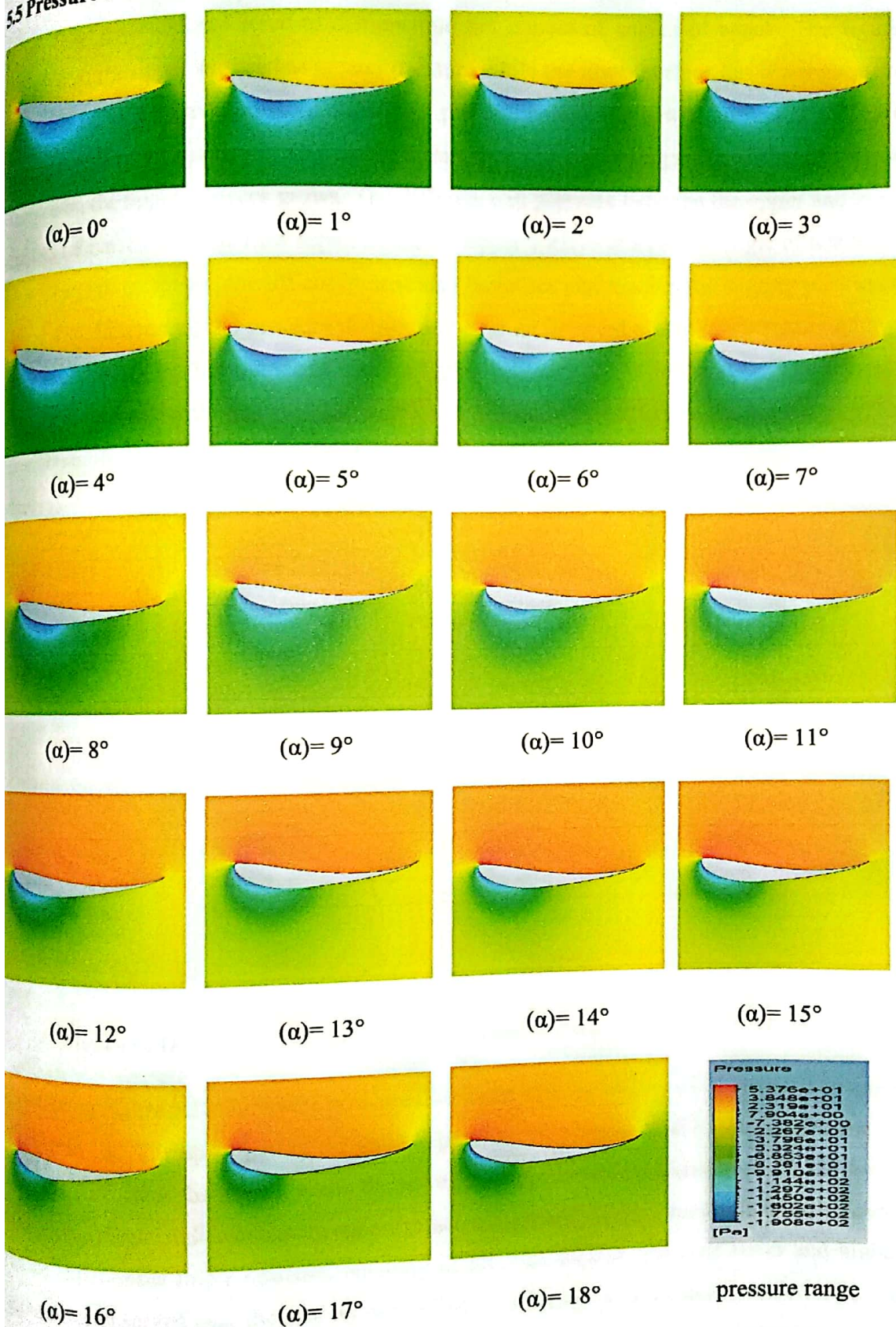
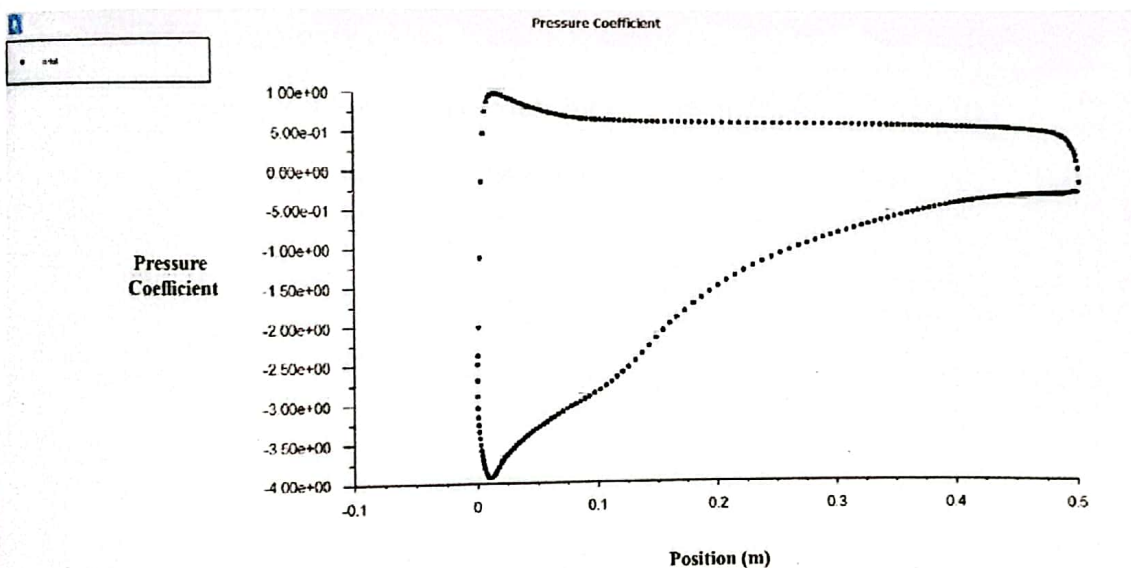


Figure 5. 17 Baseline airfoil's pressure contours for various angles of attack ( $\alpha$ )

Pressure distribution for varying angles of attack is shown in Fig. 5.17. Rather than rotating the airfoil, flow direction is altered to demonstrate the impact of angles of attack. The figures indicate that the upper surface has greater pressure while the lower surface has lower pressure. Additionally, a negative pressure region is present below the lower surface that nearly encompasses the entire surface. This region diminishes with increasing angle of attack, whereas pressure on the upper surfaces grows. The difference in pressure between the upper and lower surfaces increases until the flow separates on the upper surface at a certain angle of attack. As angle of attack increases, the lift coefficient also increases and reaches the stalling position at around  $13^\circ$ . In general, the pressure distribution over an inverted airfoil is characterized by a lower pressure on the bottom surface and a higher pressure on the top surface. The pressure gradient is steeper on the top surface, which results in a higher lift coefficient. However, the inverted aerofoil also generates more drag due to the flow separation that occurs at the trailing edge.



**Figure 5.18** Pressure coefficient on the airfoil surface at  $13^\circ$  angle of attack

The graph in Figure 5.18 shows the pressure distribution on the surface of an airfoil at an angle of attack of  $13^\circ$ . The upper part of the graph represents the pressure coefficient distribution on the upper surface of the airfoil, while the lower part represents the distribution on the lower surface. The results indicate that the upper surface experiences higher pressure, while the lower surface experiences lower pressure, resulting in lift. The highest levels of lower and higher pressure are observed near the leading edge of the lower and upper surface, respectively, and decrease towards the trailing edge.

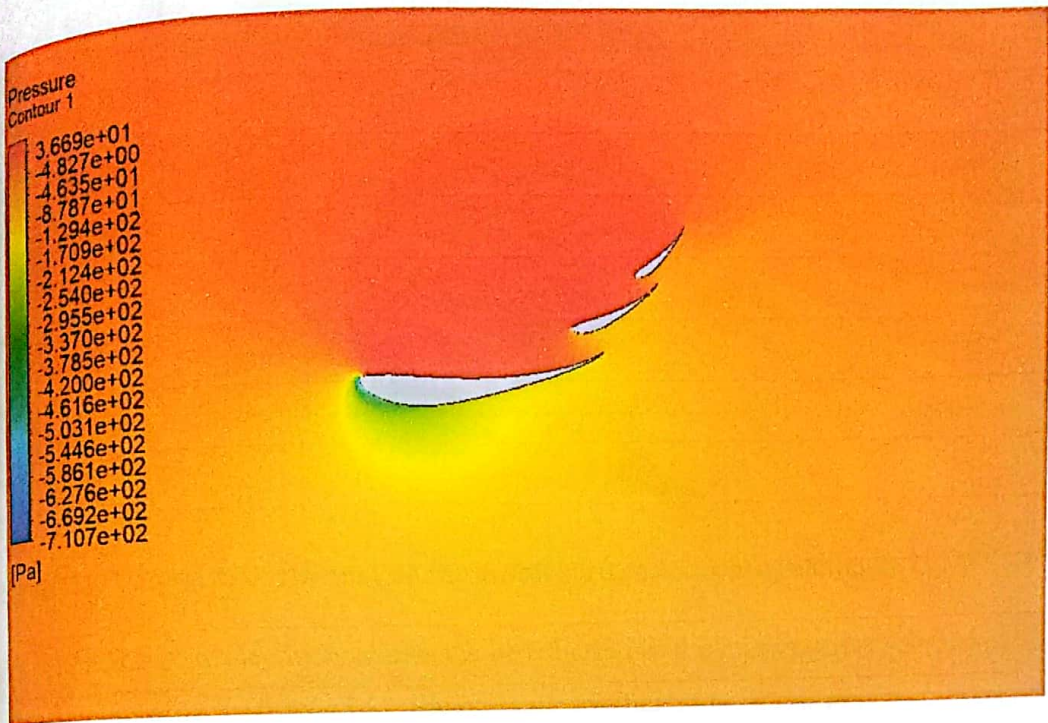


Figure 5. 19 Pressure contours for configuration A( $7^\circ, 28^\circ, 46^\circ$ )

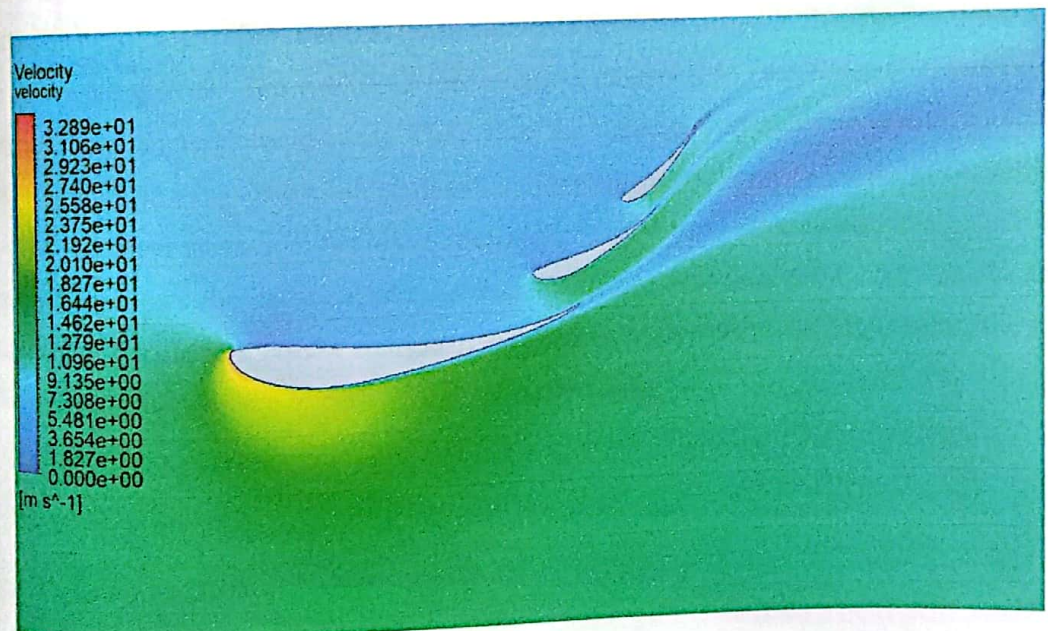
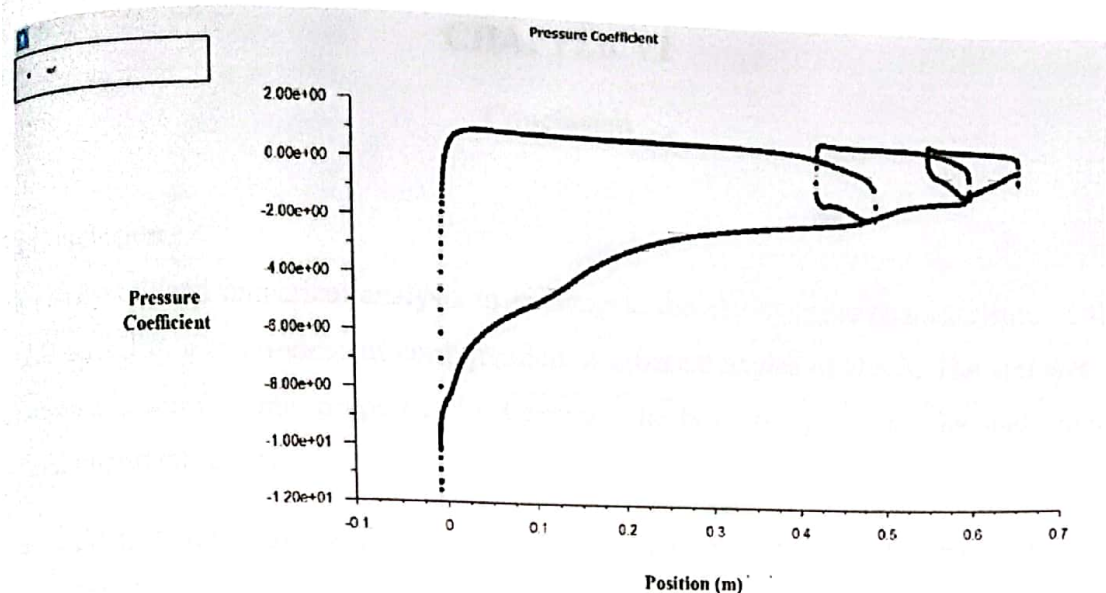


Figure 5. 20 Velocity contours for configuration A( $7^\circ, 28^\circ, 46^\circ$ )



**Figure 5. 21** Pressure coefficient on the airfoil surface for configuration A( $7^\circ, 28^\circ, 46^\circ$ )

Figure 5.19 and 5.20 respectively shows the distribution of the pressure and velocity of the air flowing over the wing. In figure 5.21, the pressure coefficient vs. location is displayed.

A multi-element wing refers to a wing design that has more than one airfoil or wing element stacked on top of each other. Each of these elements produces lift, which is the force that keeps the car on the ground. The multi-element wing is designed to create more downforce and compared to a single-element wing. They alter the velocity and pressure distribution of the airflow around the wing. The multi element configuration of the wing cause the airflow to slow down on the upper surface of the wing, increasing its pressure. This results in a negative lift force, which allows the car to generate more downforce and improve its grip on the track. Additionally, the elements cause energising the boundary layer at the trailing edge of the wing. Which in turn increases the overall efficiency of the wing.

## CHAPTER VI

### Conclusion

#### 6.1 Conclusion

This study utilized numerical analysis to investigate the aerodynamic characteristics of the S1223 airfoil in a multi-element configuration at different angles of attack. The aim was to compare the aerodynamic properties to determine the best configuration. The study found several important results:

- i. First, stalling was observed to occur for the single S1223 airfoil at an angle of attack,  $(\alpha)= 13^\circ$
- ii. Second, the multi-element configuration showed improved aerodynamic properties at low angles of attack.
- iii. Third, even though the drag increased, using a multi-element configuration was significantly more efficient for generating negative lift compared to using a single element airfoil.
- iv. Fourth, the most suitable configuration for a multi-element configuration was determined by comparing  $C_L/C_D$  ratio, negative lift coefficient, negative lift, drag, and drag coefficient at different velocities can be considered A( $7^\circ, 28^\circ, 46^\circ$ )
- v. Finally, the study analysed the pressure and velocity distribution for each case.

In summary. The study's results provide insights into understanding the design of multi-element setup for airfoils for better aerodynamic performance.

There are numerous approaches to expand the study in future. The future recommendations are:

- i. 3D flow simulation can be carried out to predict lift, drag, and other aerodynamic properties under different flight conditions and configurations.
- ii. Studying unsteady flow phenomena, such as vortex shedding
- iii. In the future, testing different airfoil geometries and configurations, such as winglets or spoilers, can be done using CFD simulations, and the most efficient design can be selected based on their performance.



## References

- [1] R. L. Fearn, "Airfoil aerodynamics using panel methods", 2008, The Mathematica Journal, 10(4), p.15.
- [2] T. Sumaryada, Jaya, A.M. and A. Kartono, "Simulating the Aerodynamics Profiles of NACA 4312 Airfoil in Various Incoming Airspeed and Gurney Flap Angle", 2018, Omega: Jurnal Fisika dan Pendidikan Fisika, 4(1), pp.1-1.
- [3] M. Grabis, R. K. Agarwal, "Computational Fluid Dynamics Analysis of High Lift, Single Element, Inv Element, Inverted Air ted Airfoils in Gr foils in Ground Effect for an FSAE Car Front Wing", 2017, Mechanical Engineering and Materials Science Independent Study. 59
- [4] R. Ma, B. Zhong, P. Liu, D. Drikakis, "Multi-Objective Optimization Design of Low Reynolds-Number Airfoils S1223", 2010, 27TH INTERNATIONAL CONGRESS OF THE AERONAUTICAL SCIENCES.
- [5] J. A. D. Ackroyd, Sir G. Cayley, "The Invention of The Aeroplane Near Scarborough at The Time of Trafalgar", 2011, Journal of Aeronautical History Paper No, p.6.
- [6] <https://www.seekpng.com/ima/u2e6r5i1e6o0q8w7/>
- [7] H. K. Versteeg, and W. Malalasekera, "An introduction to computational fluid dynamics: the finite volume method", 2007, Pearson education.
- [8] M. S., Selig and Guglielmo, J. J., "High-Lift Low Reynolds Number Airfoil Design", June 1994, AIAA Paper 94-1866,
- [9] Y. Cengel and J. Cimbala, 2012. Fluid Mechanics Fundamental and Application Third Edition.
- [10] [https://upload.wikimedia.org/wikipedia/commons/9/9c/Airfoil\\_lift\\_and\\_drag.svg](https://upload.wikimedia.org/wikipedia/commons/9/9c/Airfoil_lift_and_drag.svg)
- [11] A. S. Reddy, A. Ur Rehman, S. Shetty, S. Vivek, "Efficient Aerodynamic System of Rear and Front Wings for an FSAE Car", (2020), RVJSTEAM, 1,2
- [12] SAE International. "2017-18 Formula SAE® Rules." FSAE Online, <https://www.fsaeeonline.com/content/2017-18-FSAE-Rules-091317.pdf>.
- [13] I. Oxyzoglou, "Design & Development of an Aerodynamic Package for an FSAE Race Car", 2017
- [14] H. Al- Kayiem and K Chelven, "An Investigation on the Aerodynamic Characteristics of 2-D Airfoil in Ground Collision", 2011, Journal of Engineering Science and Technology, 6 (3), 369-381.
- [15] A. J. Peters, N. Moore and P. A. Wilson, "An investigation into wing in ground effect airfoil geometry", 2002, Proceedings of the Symposium on Challenges in Dynamics, System identification, Control and Handling Qualities for Land, Air and Sea Vehicles, Paris, France.
- [16] H. Dahlberg, "Aerodynamic Development of Formula Student Race Car", 2007, Master's Thesis, KTH Mechanics University,



- [17] S. Wordley, J. Saunders, "Aerodynamics for Formula SAE: Initial design and performance prediction", 2006, Proceedings of the SAE World Congress and Exhibition, Detroit, U.S.A
- [18] Z. Deng, S. Yu, C. Wu, "Numerical Simulation and Analysis for Aerodynamic Devices of FSAE Racing Car", 2020, J. Phys.: Conf. Ser. 1600 012079
- [19] F. Mariani, C. Poggiani, F. Risi, L. Scappaticci, "Formula-SAE Racing Car: Experimental and Numerical Analysis the External Aerodynamics", Energy Procedia 81 (2015) 1013-1029, 69th Conference of the Italian Thermal Machines Engineering Association, ATI2014
- [20] S. Hetawal, M. Gophane, B.K. Ajay, Y. Mukkamala, "Aerodynamic Study of Formula SAE Car", Procedia Engineering 97 (2014) 1198 – 1207, 12th Global Congress on Manufacturing and Management, GCMM 2014
- [21] J. Iljaž, L. Škerget, M. Štrak, J. Marn, "Optimization of SAE Formula Rear Wing", 2016, Strojniški vestnik - Journal of Mechanical Engineering 62(2016)5, 263-272
- [22] A. Verhoff, D. Stookeysberry, and S. Agrawal, 1992. Farfield computational boundary conditions for twodimensional external flow problems. AIAA journal, 30(11), pp.2585-2594.
- [23] E. Mollica, A. Timmoneri, "CFD analysis of the low Reynolds S1223 airfoil", 2021, International Journal of Engineering, Science and Technology Vol. 13, No. 4, pp. 46-49
- [24] A. M. Patil, V. S. Hole, S. S. Patil, R. R. Kharat, "Design and Manufacturing of Aerodynamic devices for Formula Student Car", April 2020, International Research Journal of Engineering and Technology (IRJET)
- [25] A. R. Hammond, R. G. J. Flay, "Aerodynamic Design of A Formula Sae Race Car", 2008
- [26] J. P. Merkel, "Development of Multi-Element Active Aerodynamics For The Formula Sae Car", December 2013
- [27] N. Rastogi, S. Shetty and B. Ashok, "Analysing the effects of air flow on a formula prototype vehicle to optimize its performance", 2017, IOP Conf. Series: Materials Science and Engineering 263 (2017)
- [28] M. A. Dharmawan<sup>1</sup>, Ubaidillah<sup>1</sup>, A. A. Nugraha<sup>1</sup>, A. T. Wijayanta<sup>1</sup>, B. A. Naufal, "Aerodynamic Analysis of Formula Student Car", 2018
- [29] S. Rehnberg, L. Börjesson, R. Svensson, J. Rice, "Race Car Aerodynamics - The Design Process of an Aerodynamic Package for the 2012 Chalmers Formula SAE Car", 2013
- [30] K. S. Lukacovic, "Innovative Rear Wing Design Research for Formula SAE", 2016
- [31] F. P. Incropera, D. P. DeWitt, T. L. Bergman, and A. S. Lavine,, 2007. Fundamentals of Heat and Mass Transfer (6<sup>th</sup> edition).
- [32] B.E. Launder, 2015. First steps in modelling turbulence and its origins: a commentary on Reynolds (1895) 'On the dynamical theory of incompressible viscous fluids and the determination of the criterion'. Philosophical Transactions of the Royal Society A: Mathematical, Physical and Engineering Sciences, 373(2039), p.20140231.



- [33] F. R. Menter, "Two-equation eddy-viscosity turbulence models for engineering applications", 1994, AIAA Journal; 32:1598-605.
- [34] A. Doosttalab, M. Mohammadi, M. Doosttalab, A. Ashrafizadeh, "Numerical Investigation of Aerodynamical Performance of Damaged Low-Reynolds Airfoils for UAV Application", 2012